Final report – Ash deposit formation and removal in biomass fired boilers. Fundamental data provided with deposit probes

Jensen, Peter Arendt; Zhou, Haosheng; Zbogar, A.; Hansen, Jørn; Jappe Frandsen, Flemming; Glarborg, Peter; Madsen, B.; Stang, H.

Publication date:
2006

Document Version
Publisher's PDF, also known as Version of record

September 28, 2006, DTU no. 50228

Energinet.DK Research PSO Project 4106

Final Report – Ash Deposit Formation and Removal in Biomass-fired Boilers. Fundamental Data Provided with Deposit Probes

Danish title: Belægningsopbygning og nedbrydning i biomassefyrede kedler. Tilvejebringelse af grundlæggende data ved hjælp af belægningsprober

Peter Arendt Jensen, Haosheng Zhou, Ana Žbogar, Jørn Hansen, Flemming Jappe Frandsen, Peter Glarborg, Birgitte Madsen, Henrik Stang

Department of Chemical Engineering
Technical University of Denmark
Building 229
DK-2800 Kgs. Lyngby
Denmark

Department of Chemical Engineering
Technical University of Denmark
Building 229
DK-2800 Kgs. Lyngby
Denmark

Energinet.DK Research PSO Project 4106

Final Report – Ash Deposit Formation and Removal in Biomass-fired Boilers. Fundamental Data Provided with Deposit Probes

Danish title: Belægningsopbygning og nedbrydning i biomassefyrede kedler. Tilvejebringelse af grundlæggende data ved hjælp af belægningsprober

Peter Arendt Jensen, Haosheng Zhou, Ana Žbogar, Jørn Hansen, Flemming Jappe Frandsen, Peter Glarborg, Birgitte Madsen, Henrik Stang

Rep.no. R0603

Table of content

Appendices

A. Task 1. Ana Žbogar, Flemming Frandsen, Peter Arendt Jensen, Peter Glarborg. Shedding of Ash Deposits – Literature review. To be submitted to Progress in Energy and Combustion Science.

B. Task 3. Ana Žbogar, Peter Arendt Jensen, Flemming J. Frandsen, Jørn Hansen, Peter Glarborg. Experimental investigation of ash deposit shedding in a straw-fired boiler. *Energy & Fuels* **2006**, 20, 512-519.

C. Task 4. Haosheng Zhou, Jørn Hansen, Peter Arendt Jensen. Measurements on sootblowing of ash deposits in a convective pass of a straw fired boiler (AVV2). CHEC report 2004. Rep.no. R0407.

D. Task 6. Haosheng Zhou, Peter Arendt Jensen, Flemming Jappe Frandsen. Dynamic Mechanistic Model of Superheater Deposit Growth and Shedding in a Biomass Fired Grate Boiler. Submitted to Fuel.

E. Task 5. Peter Arendt Jensen, Birgitte Madsen, Peter Glarborg, Henrik Stang. Sintering of biomass ash deposits. To be submitted to Energy & Fuels.

F. Task 6. Haosheng Zhou, Jørn Hansen, Peter Arendt Jensen. Resume of the report: Controlled sootblowing removal of deposits in the convective pass of a straw fired boiler.

G. Task 6. Haosheng Zhou, Jørn Hansen, Peter Arendt Jensen. Report: Controlled sootblowing removal of deposits in the convective pass of a straw-fired boiler.

H. Task 7. Haosheng Zhou, Jørn Hansen, Peter Arendt Jensen. Report: Measurements of the formation and removal of deposit in the Herning wood-oil grate combustion boiler.

1.0 Introduction

As part of the Danish policy to reduce net CO_2 emission from electricity production, biomass in the form of straw and wood is used as fuel on CHP grate boiler plants. Compared to coal, straw is a troublesome fuel with a high potassium and chlorine content that causes increased problems with ash deposit formation and corrosion of boiler tubes. Since the late 80s straw has been used in CHP grate boilers in Denmark and a lot of development has ensured that deposit and corrosion problems in such boilers in most cases are manageable, and at the same time a reasonably high superheater temperature can be used. However, even today many problems occur occasionally with boiler ash deposits that are difficult to remove. The most troublesome deposits in straw-fired boilers are often observed on two parts of the boilers, on the high temperature superheater tubes and in the top of the second draught. The deposit on the superheaters in the boiler chamber is removed mainly by deposit surface melting, while deposits removal in the convective pass in the top of the second draught can be strongly sintered and difficult to remove. Further downstream in the convective pass the heat transfer surfaces and the flue gas temperatures are so low that the deposit is often loose and easy to remove. While the deposit formation process has been the objective of several studies, only limited knowledge is available on the biomass ash deposit removal process. The present project was started to provide more detailed knowledge of the ash deposit removal process in biomass-fired boilers with the following main objectives:

- To provide improved fundamental data on deposit formation and removal and heat transfer in biomass-fired boilers
- To provide measuring data that can be used for verification of a model of deposit formation and shedding as a function of local conditions
- To provide recommendations on how deposit formation in boilers using alkali rich fuels can be minimized

The core part of the project work has been done by using an advanced deposit probe to perform measurements in straw-fired boilers, so that information on the deposit removal process was obtained near the high temperature part of the superheaters and in the convective pass in the top of the second draught.

The work in this project has been coordinated with the Eltra PSO 3144 project run by Elsam A/S (now Dong Energy): 'Optimering af belægningsdannelse i biobrændselsfyrede kedler' (Reference 1). The PSO project 3144 has mainly dealt with collection of practical experiences from literature and boiler operators, while this project has dealt with boiler probe measurements, fundamental ash deposit properties and model development.

The project work was divided into seven work tasks as follows:
Task 1. Shedding of ash deposits – literature review
Task 2. Construction of an advanced deposit probe
Task 3. Ash deposit shedding on superheaters in a straw-fired boiler
Task 4. Dynamic model of superheater deposit growth and shedding
Task 5. Biomass ash sintering
Task 6. Sootblowing experiments in the convective pass of a straw boiler
Task 7. Deposit measurements at Herningværket

A summary of the work carried out under each of the individual tasks will be presented below. Complete details are found in the reports and articles presented in the appendices. Some parts of the project work were conducted by Master of Science students doing their final project (see references 2 to 3). Thus Alfonso Modrego Marco, Ana Žbogar and Birgitte Madsen obtained their Master of Science degrees in chemical engineering.

2.0 Task 1. Shedding of ash deposits – literature review

The objective of the literature review was three-fold: 1) to review the present knowledge of deposit removal and shedding mechanisms, 2) to outline the different approaches to model these mechanism, and 3) to provide descriptions of the chemical, mechanical, and thermal properties of ash deposits. The review focused attention on biomass combustion conditions, but also the experiences from the coal-firing systems and kraft recovery boilers were taken into account.

Boiler ash deposits formed on heat transfer surfaces can increase the boiler operation costs, reduce the boiler thermal performance and in severe cases, completely plug the flue gas passages and lead to unscheduled costly boiler shutdowns. Effective deposit removal is therefore critically important in order to ensure efficient boiler operation. Deposit shedding can be defined as the process of deposit removal from the heat transfer surfaces. Mechanical devices for deposit removal such as sootblowers can be implemented into the boiler, which is often then referred to as artificial shedding. Soot-blowers use a pressurized fluid (often steam or air) to cause a mechanical and/or thermal shock that causes a failure in the deposit. On the other hand, shedding can be caused without any operational or mechanical influence by erosion, gravity shedding (including surface melting), or simply by a thermal shock.

As presented in Table 1 the locations where the removal of deposit material takes place and the type of removal mechanism may differ depending on the position in the boiler, the boiler operation, the local temperature and the deposit ash properties. The deposit removal may takes place on the deposit surface, the deposit tube interface and inside the deposit. (A) Deposit removal by erosion may take place when non-sticky fly ash particles (mainly quartz) collide with non-sticky areas on a deposit surface. (B) Gravity shedding is caused by the gravity force (deposit weight), which acts on the deposit. When the gravity force exceeds the tube adhesion strength or the deposit tensile strength the deposit will fall off the boiler tubes. (C) Another form of gravity shedding is deposit removal by

surface melting. If the temperature is high and the deposit melts at a low temperature the deposit can be removed by melt that runs down on boiler walls or superheaters. (D) Thermally induced shedding is caused by temperature changes and differences in the thermal expansion coefficients of tube and deposit or different thermal expansion coefficients of adjacent deposit layers. This may cause an uneven expansion that leads to deposit fracture. Local temperature changes can be caused by load changes or sootblowing. (E) Mechanically induced tension in the deposit may be caused by vibrations, rapping gears or sootblowers. A sootblower jet impact can cause high internal stresses in the deposit, which may lead to internal deposit break-up or debonding from the boiler surface.

Table 1. Different deposit shedding mechanisms

Deposit removal mechanism		Where the deposit sheds		
		Tube deposit interface (debonding)	Within the deposit	Surface removal
A	Erosion			X
B	Gravimetric (solid deposit)	X	X	
C	Gravimetric, surface melting			X
D	Thermally induced tension a) by combustion fluctuations b) by load changes c) by sootblowing	X	X	
E	Mechanically induced tensions a) (Natural) mechanical fluctuations b) Sootblowing	X	X	

The experimental straw boiler investigations of shedding were conducted near the high temperature part of the superheaters (task 3) and in the convective pass in the top of the second draught (task 6). Near the superheaters the shedding was caused by surface melting (C), and deposit removal in the convective pass was caused by sootblowing and both deposit fractures and debonding were observed (E).

The main focus of the literature study (task 1) was on the process of ash deposition and shedding in biomass boilers, but also deposit formation and physical properties of biomass ash deposits were reviewed. The general conclusion is that the fundamental knowledge of deposit shedding in biomass boilers is limited. Some data exist for shedding of coal deposits, while the shedding of deposits in kraft recovery boilers was systematically studied. Due to the kraft boiler specific deposit composition (consisting solely of alkali salts), the data from the kraft recovery boilers cannot be straightforwardly used, but they can be used as a starting point for future studies. The knowledge of the deposit properties, relevant to the deposition and shedding processes, and their modeling is limited. In many cases material data and models for ceramic materials have to be applied.

3.0 Task 2. Construction of an advanced deposit probe

An advanced shedding probe consisting of a horizontal cooled tube was constructed to make it possible to perform well controlled deposit formation and shedding measurements in full-size power plant boilers. The complete probe system made it possible to conduct simultaneous measurements of deposit weight, probe heat uptake, and local flue gas temperature, as well as register the deposit development by a video camera. In some experiments a sootblowing probe was also used that could expose the deposit probe to a jet of pressurized air with a known PIP (Peak Impact Pressure). In some cases the deposit probe measurements were supplemented with suction pyrometer, particle sampling and velocity measurements.

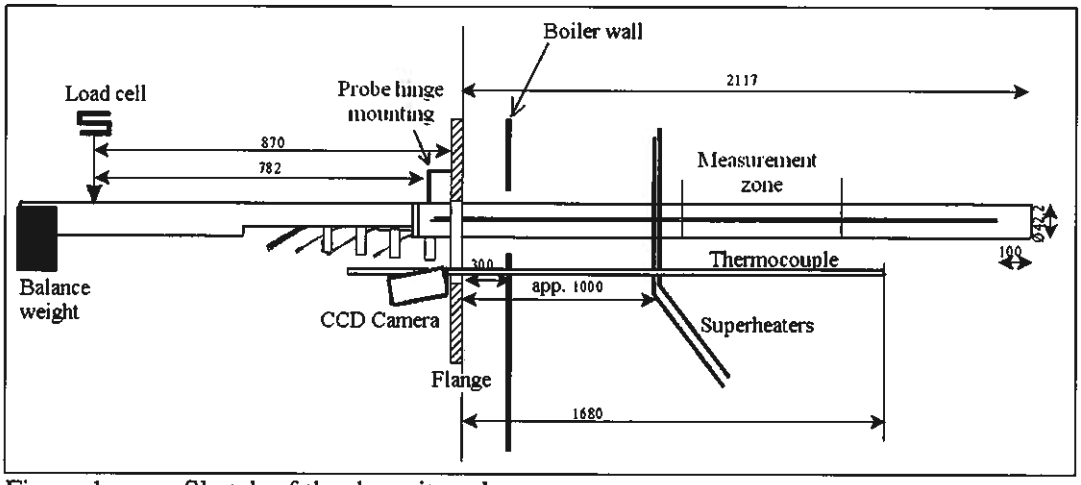

Figure 1. Sketch of the deposit probe system.

The scheme of the typical experimental probe set-up is shown in Figure 1. The probe is constructed as a double annular tube, made of stainless steel, which is cooled with counter-current flows of water and compressed air. This cooling arrangement ensures a reasonable uniform surface temperature along the whole length of the probe. Thermo-elements are placed in the outer steel tube to measure the probe metal surface temperature. The heat transfer to the probe is calculated by using measurements of the flows and the inlet and outlet temperatures of cooling water and air respectively. The mass change due to the deposit is measured by use of a load cell on which the probe hangs. The probe is fixed in position by a hinge placed adjacently to the boiler wall and the load cell as seen in Figure 1.

The probe system was applied to measurements at the Avedøre straw-fired grate boiler both near the superheaters and in the convective pass. The probe system was also applied to measurements on the Herning wood- and oil-fired grate boiler. Further details on the probe design are found in appendices B and G.

4.0 Task 3. Ash deposit shedding on superheaters in a straw-fired boiler

The deposit probe was applied to shedding measurements in the boiler chamber of the straw-fired Avedøre grate boiler, in the top of the furnace, close to the pendant superheater. An example of a video image of the probe with deposit is shown in Figure 2. The shedding probe 55 minutes after it had been fully inserted into the boiler is seen. An approximately 40 mm large straw particle can be observed, which was the largest particle observed to impact on the probe. Also two ash droplets can be seen and this was the first time that a visually observable melt appeared.

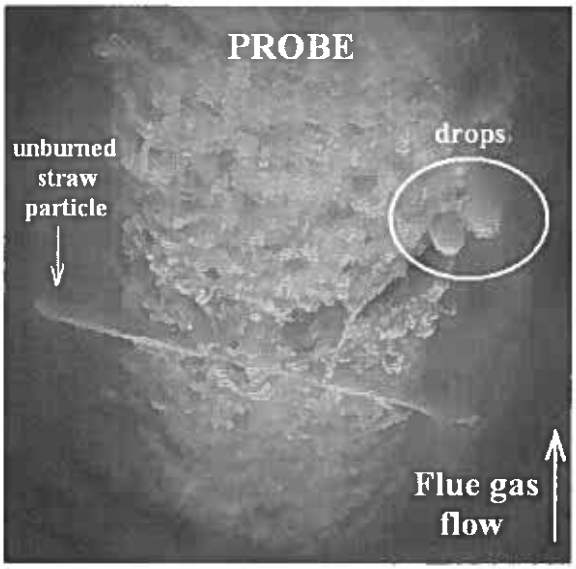

Figure 2. Image of the shedding probe 55 minutes after insertion into the boiler (T_{fg}=980^{0}C).

The aim of the conducted probe study was to investigate the process of natural ash deposit shedding in the superheater area of a straw-fired boiler. Heat uptake, mass change measurements and video recording of the ash deposit build-up process were conducted. The probe metal surface temperature was fixed at 500°C. The probe was placed for 18 days in the Avedøre straw-fired boiler, and the local flue gas temperature of 800°-1100°C caused melting to be the main deposit shedding mechanism. The probe deposit mass increased steadily for the first six days, while after day 7 the mass fluctuated up and down with a mean value of 4.5 kg (equal to 20 kg/m2). The flue gas temperature governs the state of the deposit, i.e. the fraction of the deposit that is melted, and consequently controls the shedding. The melting and partial solidification of the deposit happen periodically, following the changes in the flue gas temperature. The deposit behavior after day 7 can be divided into different regimes, depending on the flue gas temperature: 1) When the temperature is approximately 1100°C or above, the deposit surface layer is completely melted and the melt runs down the probe and a fast reduction in the amount of deposit on the probe is observed. 2) Around 1000°C the deposit contains both melt and solid particles and the deposit formation rate and the deposit shedding rates are

approximately at a similar level. 3) At 900°C and below a solid porous particle rich deposit is present on the probe and the deposit formation rate exceeds the deposit shedding.

The present investigation shows that if superheaters in straw-fired boilers are constructed so that a thick layer of deposit can be accepted, a stable deposit removal process by ash surface melting can be established. With the knowledge that at flue gas temperatures exceeding 900°C shedding by ash surface melting takes place, it is clear that sootblowing is not needed at a flue gas temperature above 900°C. Further details on the experimental study of deposit surface melting induced shedding are found in appendix B.

5.0 Task 4. Dynamic model of superheater deposit growth and shedding

A dynamic mathematical model of ash deposit growth and shedding on a horizontal cooled probe in a straw-fired boiler was developed and validated. The model includes sub-models of deposition (impaction, thermophoresis, Brownian and eddy diffusion, and condensation) and shedding by deposit surface melting. Three new sub-models describing deposit formation on the downstream side of the probe, ash droplet formation and detachment, and a correlation of ash melt fraction as functions of temperature and ash chemical composition have also been developed.

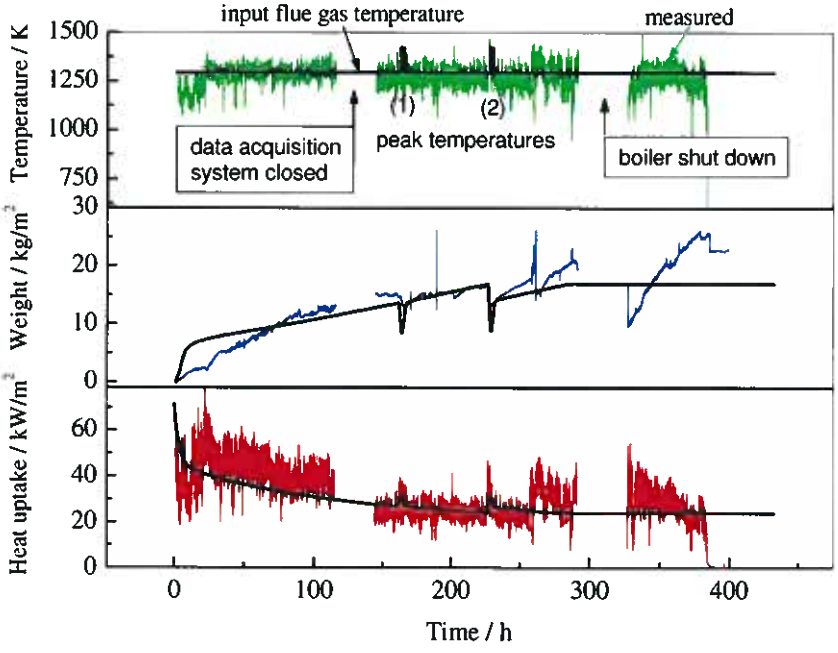

Figure 3. Evolution of the deposit weight and the heat uptake as a function of time. Comparison of measurements and model data.

The model was validated by using the measuring data obtained at Avedøreværket (see Chapter 4). Measured flue gas temperature, ash particle size distribution as well as chemical composition of the fly ash were used as input parameters to the model calculations. Figure 3 shows the measured and the calculated deposit weight and the heat uptake as a function of time, as well as the measured and the applied input temperature. Generally, the predictions are in reasonable agreement with the measurements. Three periods can be distinguished in Figure 3, i.e. a fast increase of the deposit weight and a correspondingly quick decrease of the heat uptake at an early stage (up to 10 h), then a slow increase of the deposit weight and a decrease of the heat uptake up to 285 h, and finally constant values of the deposit weight and the heat uptake appear. A sharp decrease of the deposit weight and an increase of the heat uptake can be observed when peak flue gas temperatures events at 1423 K were used (at 160 and 220h).

In general, the mechanistic model predicted reasonably well the measured probe deposit weight, the heat uptake, as well as the shape of the deposit. The simulated elliptical deposit shape on the upstream side and the very small amount of the downstream deposit after 3.5 h are in agreement with the measurements. Both the simulations and the measurements indicated that under stable boiler operation conditions, the deposit weight increases until a steady state condition is obtained where similar shedding and deposit formation rates are reached. The evolution of the deposit formation on the probe has three distinct stages: a fast increase of the deposit weight and correspondingly a quick decrease of the heat uptake at an early stage, then a slow increase of the deposit weight and decrease of the heat uptake, and finally stable values of the deposit weight and the heat uptake. KCl condensation is the main contribution to the ash deposit initiation and particle impaction is the main contribution to the deposit growth after the initial innermost layer formation. The ash deposition by large eddy dispersion on the downstream side of the probe contributes to a slow increase of the deposit weight after the shedding starts. High peak flue gas temperature events lead to a sharp decrease of the deposit weight and an increase of the heat uptake.

A detailed parametric study quantified the influence of changed local conditions on the deposit formation process. The calculation showed that the particle size, the melt fraction of ash, and the flue gas temperature have significant impact on the dynamic deposition formation process, the deposit weight, and the heat uptake. A higher flue gas temperature gave less deposit weight and a higher heat uptake. A smaller particle size made less particles impact the probe, which reduced the initial deposition rate. Further details on the model development and the parameter study are found in Appendix D.

6.0 Task 5. Biomass ash sintering

The strength of deposits is influenced by sintering that can be defined as a process in which particles grow together to a denser body. Because of the high salt content of biomass ashes deposit sintering is mainly caused by melting of the salt fraction of the ash. The deposit strength is an important parameter when deposits are be removed by sootblowing. In this study the strength development of biomass ash as a function of

temperature was investigated in the laboratory. Fly ash from a straw-fired grate boiler and fly ash from suspension firing of straw were pelletized and the compression and the bend strength were measured. The results were compared with literature data, and the strength measurements were supplemented with other investigations such as SEM images of the heated pellets. Figure 4 shows an example of some of the compression strength measurements. The compression strength of fly ash from suspension firing of straw (D) is compared to the strength of grate boiler fly ash (A). It is seen that the compression strength of fly ash (D) is largest, and also that the initial sintering starts at a higher temperature for the suspension firing ash. The suspension firing fly ash (D) contains much more silicon and calcium and less chlorine and potassium. The compression strength decreases at high temperatures, where the pellets experience a mass loss and an increased porosity that lowers the strength. The increased porosity is caused by KCl evaporation.

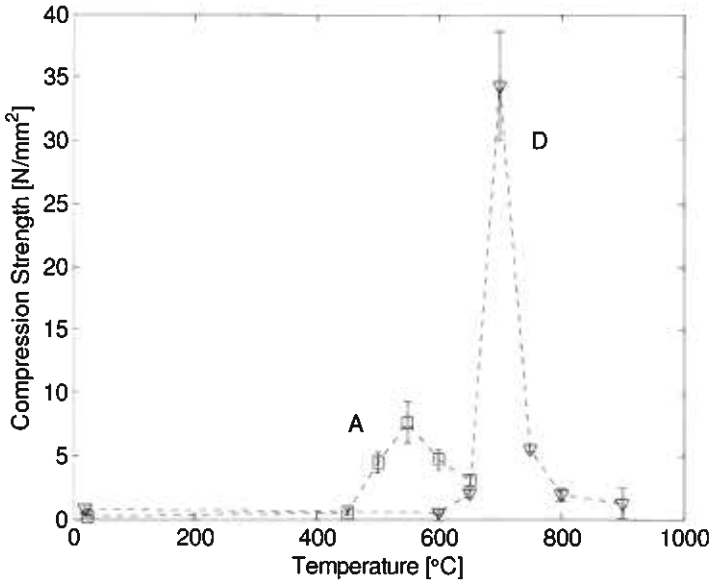

Figure 4. Compression strength of sintered fly ash from suspension firing of straw (D) and of sintered fly ash from a straw-fired grate boiler (A).

The main conclusions of the sintering study are summarized here. It is often observed that at a given temperature a steep increase in the strength of the lab ash pellets appears, and then at a higher temperature a large decrease of the strength takes place. The strength increase is related to melt formation in the sample, however, some strength increase seems to appear before initial melting of the sample. The strength decrease at higher temperatures is caused by volatilization of some ash components. A sintering temperature T_{sint} is defined as the temperature where the compression strength increases above 2 N/mm2 and the strength further increases with increased temperature. The sintering and the strength development of an ash are influenced by chemical composition, ash particle size, sintering time and probably also the flue gas composition. The measured sintering

temperatures (T_{sint}) of the investigated ashes and literature data make it possible to observe the following general trends:

- For very alkali rich ashes dominated by K, Na, S and Cl with only a low content of Si and Ca, such as some straw fly ash or ash from kraft recovery boilers, T_{sint} values from 370° to 470°C are observed. However, real biomass boiler deposits nearly always contain some Ca and Si.
- Straw and grass rich deposit ashes rich in Si and K have T_{sint} values between 610° and 710°C.
- For wood and other types of biomass ashes rich in both Si, K and Ca, T_{sint} values from 780°C and above are observed.
- Coal (bituminous) and coal straw co-firing ashes (maximum 20% straw share on an energy basis) have T_{sint} values of 920° to 1010°C.

Both the present sintering study as well as the ones found in the literature are based on laboratory measurements, and this complicates the transfer of data to boiler conditions. Long-time sintering as in boilers may be different from short-time sintering in the laboratory for several reasons. The long residence time may increase the amount of crystalline particles and decrease the amount of amorphous material. The very large pores seen in some of the laboratory samples may to some degree collapse or be filled with condensed phase ash.

Sintering of ash is still an area with many unknowns. Some important areas are the relation between compression and tensile strength, the influence of long sintering time on the strength development and the influence of the temperature at which the strength is measured. Further details on the sintering study are found in appendix E.

7.0 Task 6. Sootblowing experiments in the convective pass of a straw boiler

The main objective of this experimental investigation was to determine the needed PIP values to remove deposits. A sootblower jet of steam or pressurized air is often characterized by the locally obtained Peak Impact Pressure (PIP). The peak impact pressure is the local stagnation pressure at the center of the sootblower jet at a given distance. The stresses in a deposit are related to the force on the deposit that is induced by the jet and the magnitude is related to the PIP value. A more sintered deposit with a high strength needs a higher PIP value to be removed.

In this study a series of well controlled sootblowing experiments was performed in the year 2005 at the Avedøre straw-fired grate power plant using an advanced deposit probe and a probe sootblower. The probe system was placed in the top of the second draught near superheater 1 where the flue gas temperature was approximately 750°C, and most of the experiments were conducted in the autumn of 2005. The ash deposit was allowed to accumulate on the deposit probe and a separate sootblower probe was used to expose the deposit to jets of pressurized air with known PIP. The influence of deposit probe residence time and surface temperature on the needed PIP values was quantified. Besides information on the removability of the deposits it was also possible to obtain information

on deposit chemistry, deposit formation rate and heat transfer to the probe. To obtain a consistent set of measuring data many supplementary investigations were conducted, such as fuel and ash sampling, flue gas velocity measurements etc.

Measuring campaigns with deposit probe temperatures from 400° to 550°C were conducted, and the total exposure time of the deposit probe in the boiler was more than 2100 h. Most of the probe equipment worked well during the measuring campaigns. However, it was not possible to use the deposit weight measurements to quantify the amount of deposit removed by sootblowing. The sootblowing events caused a change in the zero point value of the weight measurements that made it impossible to determine accurately the weight change caused by sootblowing. The influence of the sootblower jets on the deposits was mainly quantified by looking on the video recordings of the front deposits.

The probe rear outer layer deposit was always removed easily and a portion of or no front outer layer deposit could be removed by sootblowing in the experiments. The removability of the deposit is therefore defined as the ratio (area, %) of the outer layer front deposit that was removed by the sootblowing. The removal of the rear and front deposits happens mainly as a powder cloud and in large 'chunks', respectively, denoting the deposit removal mechanisms by fracture and debonding.

Table 2. Removable fraction of probe deposit by plant sootblowing and the PIP values needed to remove the deposits.

Probe metal temp. (°C)	General comments	Plant sootblowing		Probe sootblowing			
		Percent of deposit removed after 100 h (%)	Percent of deposit removed just before the probe was taken out (%)	PIP[*1] needed to remove deposit after 100 h (kPa)		PIP needed to remove deposits just before the probe was taken out (kPa)	
				<25 %	>75%	<25%	>75%
400 A[*3]	Deposits (outer layer) removed easily	100	100	No controlled sootblowing			
400 B	Deposits (outer layer) removed easily	100	100	<0.5[*2]	<0.5	<0.5	<0.5
450	The removable fraction decreases with increasing probe exposure time	0	Some	0.5	15	1.2	30
500 A	The removable fraction decreases with increasing probe exposure time	100	0	5	35	25	116
500 B	The removable fraction decreases with increasing probe exposure time	The probe was in the boiler for only 72 h		The probe was in the boiler for only 72 h and no controlled sootblowing was done			
550	No deposit can be removed 24 h after the probe has been exposed in the boiler	0	0	No deposits can be removed by sootblowing 24 h after the probe has been in the boiler			

*1 The PIP is the measured value at room temperature.
*2 The supplying air pressure is less than 0.2 bar.
*3 This campaign was conducted in the year 2004.

In Table 2 the results regarding the removability of deposits at different probe temperatures are summarized. The table shows the removed fraction of the front outer layer probe deposit by plant sootblowing, and the sootblowing probe PIP needed to remove a small (< 25 %) or a large (> 75 %) fraction of the probe deposits. A larger fraction of the deposit could be removed after a boiler stop, but the measurements indicated that the later boiler shutdowns were less beneficial.

It was generally observed that increased residence time or probe temperature meant that less front outer layer probe deposit could be removed. At a probe temperature of 400°C all deposit could be removed, even at moderate PIP values. At 450°C and 500°C the needed PIP increased with time, and at 550°C, even with the maximum available peak impact pressure of 190 kPa, no deposit could be removed.

Besides the quantification of the PIP pressures needed to remove deposits a lot of other valuable information was obtained. Examples of some results are listed here:

- By use of the probe weight measurements the deposit formation rate between sootblowing events could be determined. The mean deposition rate seems to be reasonably independent of the probe temperature and was measured to be from 30 to 45 g/m^{2}h in the year 2005.
- The influence of the sootblowing on the heat uptake depends on the probe temperature. At probe temperatures of 500 °C and 550 °C the heat uptake initially decreases, but levels off around 6 and 4 days after the probe has been placed in the boiler, while the heat uptake capability keeps constant at a probe temperature of 400 °C. The heat transfer level to the probe right after sootblowing is reasonably independent of probe temperature (2005 measurements, mainly 30 to 40 kW/m^2) except in the cases of high probe temperature and long residence time, where lower values are observed.
- The probe temperature significantly affects the deposit porosity, such that porosity is high at 400°C but significantly lower at higher temperatures.
- As compared with the concentrations of the elements in the fly ash, the front deposits are rich in the nonvolatile elements Ca and Si. A tendency to less chlorine in the high temperature probe deposits is observed.

Further details on the sootblowing experiments are found in appendices C, F and G.

8.0 Task 7. Deposit measurements at Herningværket

Probe measurements on the formation and removal of probe deposit have been performed at the Herning wood- and oil-fired grate boiler. Only limited information was obtained due to several problems with the experimental equipment. Problems appeared both with the video equipment, the heat transfer measurements and the weight cell. The reason seems to be that the probe was placed near a sootblower that impacted the probe with a very high force during sootblowing events. Of the few data obtained the following should be mentioned:

- The deposits were dominated by Ca, K and Si and only low concentrations of Cl. Ca, Si and Mg were enriched compared to the fly ash in the front deposit.
- A relatively low deposit formation rate of 1.45 g/(m^2h) was measured on the probe.

9.0 Conclusion, technical implications and further work

This Energinet.dk funded project has provided a broad range of information on ash deposit removal in straw boilers as well as knowledge of deposit formation and sintering. The project work has included a literature study, development of a model of shedding of high temperature deposits by surface melting and deposit probe measurements in biomass-fired boilers. The probe measurements were conducted both in the boiler chamber and in the convective pass of the Avedøre power station straw-fired grate boiler as well as in the Herning wood- and oil-fired grate CHP boiler. The main project results have been summarized in chapters 2 to 8 in this report.

The practical technical implications of the large amount of scientific data can be difficult to overview. We recommend that power plant and boiler engineers who want to utilize the results contact some of the authors. However, two short examples of the implications of the project results shall be discussed here.

The deposit on pendant superheaters in straw-fired boilers is removed by deposit surface melting. If the superheaters are designed with a sufficient tube or plate distance so that a layer of deposit up to 10-15 cm thick can be present, then it can work well. The conducted measurements indicate that if this method shall work the flue gas temperature shall be in the range of 900° to 1100°C. If the flue gas temperature is below 900°C the deposit cannot be completely removed by surface melting, and other deposit removal methods should be used. If the flue gas temperature is above 1100°C only a thin layer of deposit will be present on the superheaters, and this will cause a very high heat transfer to the tubes. The high heat transfer may be a problem if the size of the superheater is designed on the assumption that a thick deposit layer is present. The dynamics of the complete boiler operation conditions on the deposit formation may be complicated. The boiler load, the fuel composition and the operation of the grate combustion strongly influence the fly ash formation process and thus the fly ash concentration. The fly ash concentration has a large influence on the time (several days) it takes before a steady state amount of deposit has accumulated on the superheater surfaces.

Sintered difficult-to-remove deposit seems to appear in the convective pass where the flue gas temperature is between 600° and 900°C. At temperatures above 900°C surface melt deposit removal can take place, and the laboratory study on sintering indicates that typical straw deposits are not strongly sintered at temperatures below 600°C. If the boiler tube temperature is maximum 450°C such convective pass deposits on horizontal tubes can be removed by regular sootblowing (one time daily ore more), if a sootblower jet with a Peak Impact Pressure of 30 kpa or above is available. If higher tube surface temperatures are used or the available Peak Impact Pressure is lower than 30 kpa other

methods may be needed to remove the deposits. This can be water sootblowing or regular boiler shutdowns and manual deposit removal. Large load changes can also assist the deposit removal process, however, when three boiler shutdowns have happened the last seems only to improve the sootblowing for a few days.

The study of biomass deposit removal processes has even on a global scale only been the scope of relatively few scientific investigations. Thus there are still many important subjects that have not been studied in detail, and some important unresolved questions are as follows:

- Sintering of ash is still an area with many unknown variables. Some important areas are the relation between the compression and the tensile strength, the influence of gas composition, the influence of long time sintering on the strength development, and the influence of temperature at which the strength is measured.
- Most shedding studies have been based on measurements in grate boilers while only limited data are available from biomass suspension firing. Also subjects like the characteristics of water sootblowing and the influence by fuel changes have not previously been studied. Moreover only limited work has been done on boiler wall deposits.
- Detailed models of deposit removal by sootblowing and water sootblowing are not available, and in many cases the availability of important physical material properties is limited.

10.0 **Danish summary**

Mens belægningsopbygning i biomassefyrede kedler har været undersøgt i en række forskellige projekter er viden om fjernelse og nedbrydning af belægninger kun i begrænset omfang undersøgt. I nærværende projekt er udført en detaljeret grundlæggende undersøgelse af biomassebelægningers fjernelse med henblik på at opfylde følgende projektformål:

- At tilvejebringe forbedrede grundlæggende data for opbygning og nedbrydning af belægninger og varmetransmission i belægninger i biomassefyrede anlæg.
- At tilvejebringe data som kan anvendes til udvikling af en model, som beskriver dannelse og nedbrydning af alkalirige belægninger som funktion af den lokale askeflux, gastemperatur og probeoverfladetemperatur.
- At udarbejde anbefalinger for hvorledes belægningsdannelse i kedelanlæg, der anvender alkali rige brændsler, kan minimeres

En stor del af projektet er gennemført via målinger med en avanceret belægningsprobe på biomassefyrede kedler. Projektet er gennemført via udførelse af syv arbejdspakker som er kort beskrevet i det følgende.

Arbejdspakke 1. Litteratur undersøgelse om belægningsfjernelse. Den nuværende viden om belægningsfjernelse og væsentlig viden nødvendig for modeludvikling er tilvejebragt.

Arbejdspakke 2. Design og fremstilling af avanceret belægningsprobe. Den avancerede belægningsprobe giver mulighed for en række samtidige målinger af probe-

og gas-temperatur, probens varmeoptag, belægningsvægt samt video monitorering af belægningsopbygningen.

Arbejdspakke 3. Undersøgelse af belægningsdannelse og fjernelse på overhederne i en halmfyret kedel. Der er udført probemålinger ved de hængende overhedere på Avedøreværkets halmfyrede ristekedel. Belægnings fjernelse ved overfladesmeltning er undersøgt og kvantitative målinger udført

Arbejdspakke 4. Udvikling af dynamisk model for opbygning og fjernelse af belægninger på overhederne i en halmfyret kedel. Modellen er verificeret med målinger fra arbejdspakke 3 og indflydelsen af ændringer i de lokale forhold er undersøgt via et parameter studie.

Arbejdspakke 5. Laboratorie undersøgelse af sintring af bioasker. Sintring egenskaberne af bioasker er undersøgt i laboratoriet. Askernes sintring har stor indflydelse på fjernelsen via sodblæsning.

Arbejdspakke 6. Sodblæsningsundersøgelse i det konvektive træk på halmfyret kedel. Ved målingerne er tilvejebragt information om det sodblæsningstryk som er nødvendigt for at fjerne belægninger opbygget ved forskellige røtemperaturer. Herudover er tilvejebragt en stor mængde informationer om belægningsegenskaber og belægningsopbygning.

Arbejdspakke 7. Belægningsmålinger på Herningsværkets træ og olie fyrede kedel. Relativt få resultater var tilvejebragt her på grund af problemer med udstyret.

De i projektbeskrivelsen opstillede mål er blevet opfyldt ved projektets gennemførelse.

Acknowledgement

The financial support under the contract PSO Eltra 4106 (now Energinet.DK) is gratefully acknowledged. Employees from the companies Elsam A/S and Energi E2 A/S have provided a lot of both technical information and support for the full-scale boiler measurements. We wish to thank Henrik Jacobsen, Henrik Frahm, Jørgen Hansen, Katrine Nielsen, Lars Fenger and Jørgen Peter Jensen, all belonging to Energi E2 A/S. Moreover, we wish to thank for the assistance from Helle Junker, Lars Wolf, Bo Sander and Peter Myrhøj belonging to Elsam A/S. The companies Elsam A/S and Energi E2 A/S are at present merged into the companies Dong Energy A/S and Vattenfall A.B. The shedding project work is part of the CHEC (Combustion and Harmful Emission Control) Research Center funded by the Technical University of Denmark, the Danish Technical Research Council, the European Union, the Nordic Energy Research program, Dong Energy A/S, Vattenfall A.B., other Danish companies, PSO funds from Energinet.DK and the Danish Energy Research program.

References

1. Lars Wolff, Helle Junker, Anton Kristiansen. Optimering af belægningsfjernelse i biobrændselsfyrede kedler – Erfaringer med belægningsfjernelse og identifikation af optimeringspotentiale. Slutrapport Eltra PSO-projekt nr. 3144. Elsam 2006.
2. Alfonso Modrego Marco. Shedding of Deposits in Biomass Fired Boilers. Master of Science thesis, January 2003. CHEC, Department of Chemical Engineering, DTU.
3. Ana Žbogar. Theoretical and Experimental Quantification of the Shedding of Biomass-derived Superheater Ash Deposits. Master of Science thesis, February 2004. CHEC, Department of Chemical Engineering, DTU.
4. Birgitte Madsen. Afkast af askebelægninger i halmfyrede kedler. Master of Science thesis, February 2005. CHEC, Department of Chemical Engineering, DTU.

Appendix A

Literature study

Shedding of Ash Deposits

Ana Žbogar, Flemming Frandsen, Peter Arendt Jensen,
Peter Glarborg

August 2006

CHEC Research Centre
Department of Chemical Engineering
Technical University of Denmark
Building 229
DK-2800 Lyngby
Denmark

List of Figures

List of Tables

List of Figures

List of Tables

Abstract

Ash deposits, formed during fuel thermal conversion, and located on furnace walls and on convective pass tubes, may seriously inhibit the transfer of heat to the working fluid, and hence reduce the overall process efficiency. Combustion of biomass causes formation of large quantities of troublesome ash deposits, which contain significant concentrations of alkali, and earth-alkali metals. The specific composition of biomass deposits gives them different characteristics as when compared to coal ash deposits, i.e. different physical significance of the deposition mechanisms, lower melting temperatures, etc. Low melting temperatures make straw ashes especially troublesome, since their stickiness is increased at lower temperatures, compared to coal ashes. Increased stickiness will eventually lead to a higher collection efficiency of in-coming ash particles, meaning that the deposit may grow even faster.

Deposit shedding can be defined as the process of deposit removal from the heat transfer surfaces. Mechanical devices for deposit removal can be implemented into the boiler, which can be then referred to as artificial shedding. Soot-blowing is one such process, where a pressurized fluid is used to cause a mechanical and/or thermal shock that would cause a failure or fissure in the deposit. On the other hand, shedding can be caused without any operational or mechanical influence by erosion, gravity shedding, or simply by a thermal shock. Which mechanism that will be dominant, depends on the ash characteristics and the boiler operation.

Different deposit characteristics will govern the ash deposit behavior, and thus the mechanism of deposit shedding. The deposit strength will influence the erosion and gravity shedding mechanisms. The ash viscosity and the melting behavior will govern the gravity shedding mechanism, while the thermal expansion coefficient will influence the thermal behavior of the deposit.

Introduction

The objective of this paper is three-fold: 1) to review the present knowledge on deposit removal, and shedding mechanisms, 2) to outline the different approaches to model these mechanisms, and, 3) to provide a simple description of the mechanical, and thermal properties of ash deposits. The review focuses attention on biomass combustion conditions, but also the experiences from the coal-firing systems and the craft recovery boilers has been taken into account. The goal of this review is to provide appropriate background information for the direction of deposit removal. Also deposit formation mechanisms are being reviewed.

One of the major operational problems in solid fuel boilers is the formation of troublesome deposits, from ash species in fuel. Ash formed during fuel thermal conversion and deposited on furnace walls and convective pass heat transfer surfaces, act as a heat transfer resistance, and may thereby inhibit heat transfer to the steam cycle. If not removed, deposits may reduce the boiler thermal performance and, in severe cases, completely plug flue gas channels and therefore subsequently cause unscheduled boiler shutdowns. Ash deposits may also cause severe corrosion of heat transfer surfaces.

Power suppliers today use biomass fuels (mainly straw and wood chips), in addition to the more traditional fossil fuels (oil, coal, and natural gas). Due to the difference in composition between straw and coal, mainly in quantities of sulfur (higher in coal), and potassium and

chlorine (higher in straw), the use of straw in combustion units is a serious technical challenge [1,2]. Danish experience shows that straw-firing causes the formation of large quantities of troublesome deposits, consisting mainly of potassium, chloride and silicates, and to a lesser extent also of calcium and phosphorus [1,3,4]. The specific composition of biomass-derived deposits gives them different characteristics, compared to coal-derived deposits, i.e. different physical and chemical structure, etc. Melt formation at low temperatures makes straw ashes especially troublesome, since it causes an increase in the stickiness of the deposit surface [3]. The appearance of a melt, and thus an increased stickiness, lead to a higher collection efficiency of the deposit toward incoming fly ash particles, meaning that the deposit may growth faster.

Effective deposit removal is important, in order to ensure a maximum boiler thermal efficiency. Deposit shedding is the process of deposit removal from a boiler surface, which can be caused artificially as a part of the boiler operation, e.g. by soot blowing, or naturally, without any operational or mechanical influence. Mechanisms of natural shedding in combustion systems are: 1) erosion, 2) gravity shedding, and, 3) thermal shock. Erosion is the process of removal of a sintered deposit by hard impacting fly ash particles, mainly silicates. Gravity shedding will occur when the gravity force on the deposit is strong enough to cause 1) break inside the deposit, or, 2) flow of molten deposit. Break inside the deposit will occur when the gravity effect on the deposit piece becomes larger compare to: 1) the force holding the deposit together (deposit strength), or 2) the force holding the deposit and the tube together (adhesion). Melting can be considered as a type of gravity shedding, where the gravity force acts on a molten deposit, forcing it to flow down the heat transfer surfaces. Thermal shock induced shedding is caused by temperature changes, due to the difference in the thermal expansion coefficients of tubes and deposits. A sudden temperature gradient (due to fluctuations of the flue gas- or steam temperature), may cause an uneven expansion of 1) deposit and tube, or, 2) distinct, adjacent, deposit layers, leading to deposit fractures.

Which mechanism that will be the dominant one, depends on the ash characteristics and the conditions inside the thermal fuel conversion system. The deposit composition will directly influence the deposit strength, the melting temperature, and the thermal expansion, i.e. the deposit properties which will affect the above mentioned mechanisms of shedding. The flue gas temperature will influence the deposit surface temperature, and thereby the temperature distribution inside the deposit. This will again influence the above mentioned deposit properties as well as the physical state of the deposit, i.e. if it is molten or solid.

Artificially, ash deposits can be removed from the heat transfer surfaces by inducing mechanical or thermal stresses inside them. This can be done using the impact of the high pressure steam, air, or water (sootblowing), by changing the thermal load, etc. Techniques for tube cleaning, implemented in the boiler operation, are practical as long as the deposits are not highly sintered or strongly attached to the surface.

Some deposits are removed immediately by soot-blowing, leaving an almost clean tube surface behind. Other deposits are difficult to remove and may leave a thin coverage of deposits, on the top of which subsequent deposition takes place [5]. Thus, an understanding of the relationship between the nature of a deposit, the thermal and mechanical properties relevant to the shedding, may improve the current – somewhat - subjective approach to the selection, location, and operation of soot-blowers, increasing thereby both the cost effectiveness, and, the availability of the unit.

The deposit formation processes has been studied thoroughly through several years, but the knowledge about deposit shedding is relatively limited. Most of the studies available in the open literature are dealing with the removal of deposits in the kraft recovery boilers [6,7,8],

which composition is somewhat different compared to biomass deposits, as will be discussed later.

1. Formation and Development of Fireside Ash Deposits

During combustion of a solid fuel, incombustible, inorganic material in the fuel is being transformed into intermediate ash species, i.e. gases, liquids and solids. The fate of the individual, inorganic element depends upon its mode of occurrence, the fuel composition, and the physical conditions within the boiler. Accumulation of ash species on heat transfer surfaces causes formation of fireside deposits.

Fire side deposits are complex, heterogeneous and porous materials which are formed on furnace walls and convective pass heat transfer surfaces, during the fuel thermal conversion process. The ash deposits may seriously inhibit heat transfer to the steam cycle.

1.1. Ash Transport Mechanisms influence on Deposit Formation

Fly ash formed during thermal fuel conversion, is carried by the flue gas down through the plant. The fly ash can be deposited on the furnace walls, and heat transfer surfaces. According to Laursen et el. [9], typical transport processes from the flue gas to the heat transfer surfaces include diffusion, thermophoresis, and inertial impaction. Possible transport mechanisms of gaseous and solid ash components to a cylinder in cross-flow are shown in Figure 1.

Diffusion is the mechanism of transport of vapors and small particles toward a solid surface, caused by a local concentration gradient. In case of Fick's diffusion molecules will move toward a solid surface due to a concentration gradient. Brownian diffusion represents the random movement of small particles, while eddy diffusion represents diffusion in turbulent systems. Once transported to the surface by diffusion of vapors can condense on or adhere to it. Condensation is a phase transformation by which vapors condense on a surface which is cooler than the local flue gas. Condensed material may increase the contact area between an otherwise particulate deposit and a surface. This may increase the difficulty of removing the deposit from the surface of the tubes [10].

Thermophoresis is a transport mechanism of small particles due to the presence of a temperature gradient. A particle suspended in a fluid within a steep temperature gradient interacts with the fluid molecules. The fluid molecules have higher average kinetic energies on the hot side compared to the molecules on the colder side. The collision of high energy molecules on the hot side of the particle has more momentum than those on the cold side, which gives rise to a net force on the particle. This force will act in the direction opposite to the temperature gradient.

Inertial impaction is the process by which the bulk of the fly ash is transported to a single tube. Due to their mass, large particles (10 μm and larger) have sufficient inertia to traverse the gas stream lines, and impact on the surface [4,11] Inertial impaction generally results in a coarse-grained deposit. The rate of inertial impaction depends on the target geometry, the particle size distribution, the particle density, the angle of impaction, as well as on the gas flow properties.

Deposits formed by diffusion and thermophoresis are evenly distributed around the tube, while the deposit formed due to inertial impaction will be formed only on the upstream tube side, and will cause an elliptic- or mountain-like-shaped upstream deposit, as shown in Figure 2 [11].

1.1.1. Overall Model for Ash Deposit Growth

The overall ash deposition process on a tube in a cross flow is illustrated in Figure 3. This figure shows the mass coming into the system by inertial impaction (diffusion and thermophoresis can also occur), and the mass leaving the system by erosion (other shedding mechanisms may also be controlling). The particles represented by open symbols are sticky; the shaded particles were sticky on arrival, but solidified in the deposit; the cross-hatched smooth particles were fused in the furnace but not sticky on arrival at the region of interest; the jagged cross-hatched particles were never completely fused and are expected to posses the highest erosivity.

A clean tube collects condensing material and sticky fly ash particles, which will solidify on the surface as long as the deposit is thin. As the deposit surface temperature increases, some particles could remain sticky on the surface even after cooling to the instantaneous surface temperature, causing an increase in the collection efficiency [12]. Deposits may be removed by erosion of a solid surface (dry deposit) by solid particles, by melting, by thermal shock, etc. Under favourable conditions the mass of deposit per unit area of tube eventually reaches a steady value at which the addition of new material is just balanced by the loss due to shedding.

Superimposed on the mass accumulation of deposit, due to diffusion, thermophoresis and inertial impaction, is the mass loss due to deposit shedding. Mass accumulation depends on the flow conditions inside the boiler, the temperature-profile in the gas film outside the deposit, and the concentration of vapours and fly ash particles, etc. Shedding is here assumed to be a function of the deposit loading on the tube (mass of deposit per unit area, m_{dep}/A_t), and occurs at a rate which may be characterised by a rate coefficient k_{shed}. As stated in Walsh et al. [12], deposit growth is the difference between the deposition and the shedding rates:

$$\frac{1}{A_t}\cdot\frac{dm_{dep}}{dt} = F_{imp}\cdot f_{dep} - k_{shed}\cdot\left(\frac{m_{dep}}{A_t}\right)^{\alpha} \qquad (1)$$

$$\text{where } \frac{m_{dep}}{A_t} = 0, \text{ at } t = 0$$

where A_t is the projected area of tube in a plane perpendicular to the undisturbed flow direction, F_{imp} [kg/m^{2}s] is the mass of ash particles impacting on the tube per unit time and unit projected area, f_{dep} is the net mass fraction of impacting particles that form the deposit, α is the order of the shedding process with respect to deposit mass per unit area, and k_{shed} [Hz] is the deposit shedding frequency when α=1. The order α of the shedding process with respect to deposit loading, depends on whether the shedding is due to external influences such as temperature fluctuations, sootblowing, and load changes; or to tensile and shear stresses arising from the weight of the deposit itself. In the study [12], where the deposition of the bitominous caol ash was investigated, α was set equal to 1.

In most real situations it will not be possible to solve equ. (1) explicitly, since the collection efficiency, f_{dep} and k_{shed} is a complicated function of the deposit loading, due to the increase in surface temperature with the increasing deposit thickness. According to equ.(1), the deposit growth was approximated by accumulating deposit in small increments, beginning with a clean tube. Under a fixed set of conditions, a steady deposit loading is approached when deposition is balanced by shedding. The loading is then found from equ. (1) by setting the net rate of deposit growth equal to zero:

$$\left.\frac{m_{dep}}{A_t}\right|_{t\to\infty} = \left(\frac{F_{imp}\cdot f_{dep}}{k_{shed}}\right)^{1/\alpha} \qquad (2)$$

This expression only applies when the deposit strength does not change, e.g. by sintering.

The net mass fraction of impacting particles which form deposited, f_{dep}, is the net result of the processes of sticking and erosion, which may occur on collision of incoming particles with particles on the deposit surface. It can be calculated using the evaluated mass-based sticking probabilities, as [12]:

$$f_{dep} = p(T_g) + \left[1 - p(T_s)\right]\cdot p_{sur}(T_s) - k_e\left[1 - p(T_g)\right]\cdot\left[1 - p_{sur}(T_s)\right] \qquad (3)$$

where p(T) is the sticking probability of incoming particles at temperature T, T_g and T_s are the gas and surface temperatures, respectively, k_e is erosivity of dry ash toward towards its deposits, and p_{sur} is the sticking probability for the particles exposed on the surface. This approach applies only to a deposit consisting of discrete particles and not to a deposit covered by slag which forms a more or less homogeneous melt.

When the fraction of impacting particles that are being deposited, f_{dep}, has been evaluated, the shedding frequency can be found from equ. (2), using an estimate of the asymptotic deposit loading from the long term measurements.

1.2. Development of Ash Deposits

The physical and chemical characteristics of the deposit are changing during the process of deposit initiation, growth and maturation, due to retention of different ash material and due to deposit consolidation. Deposit development occurs through the process of deposit sintering.

1.2.1. Sintering of Ash Deposits

During the deposit consolidation, a process known as sintering occurs. Sintering is the term commonly used for describing particle-to-particle attachment during heating, which causes increased contact between the ash particles. The driving force for sintering is the surface energy of the involved particles, i.e. densification by sintering leads to a decrease in surface area between the condensed phase and gas, and thereby the surface energy, as solid-vapor interphases are replaced by solid-solid (or liquid) interphases with lower energy [13].

Sintering may occur by several mechanisms [14]. *Liquid state sintering* causes sintering through the appearance of melt. The amount of melt formed controls the rate of neck formation between the particles. Liquid state sintering may involve a viscous liquid (e.g. melted silicates), and is typically referred to as viscous flow sintering. The essentials of liquid-phase sintering in multi-component aluminosilicates can be deduced from phenomenological observations of densification and shrinkage [15]. *Chemical reaction sintering* occurs when a reaction between the particles leads to the formation of a third component, which forms the necks between the particles. In *solid state sintering*, where densification is achieved through changes in particle shape, may occur through several mechanisms. Material may be transported to the neck area by: 1) diffusion along the particle surface, 2) diffusion through the interior of particles, or 3) diffusion through the surrounding gas phase by vaporization and subsequent condensation.

Sintering leads to the increased contact between the ash particles in a deposit. Unsintered deposits consist of distinct particles that appear isolated from their neighbors, or

with only weak particle-to-particle contact. When the deposit is sintered, the solid phase is interconnected and forms a large plate-like feature near the outside surface of the deposit.

Scanning Electron Microscopy (SEM) analyses indicate that biomass ash deposits have a layered structure with a relatively unsintered, innermost layer [16]. The initial layer, adjacent to the heat transfer surface (colder comparing to the surrounding flue gas), usually has particulate structure, consisting of a continuous gas phase and discrete solid particles. Due to its structure, thermal conductivity of this layer is low, causing poor heat transfer and thereby increasing the deposit outer layer temperature. According to Robinson et al. [16], this inner layer largely determines the overall deposit thermal conductivity. On the other hand, due to higher surface temperatures, the outermost layer can be completely fused with gas pockets embedded in the solid continuous phase.

Concerning the deposit removal process, the major importance of sintering is its influence on the deposit strength build-up. Deposit strength is often more important for successful boiler operation than the rate of deposit build-up, due to its direct effect on the ash removability by sootblowing [15].

1.2.1.1. Densification

Densification of deposits occurs through filling of a large fraction of the deposit pores by liquid [15]. Figure 4 shows the dependency between the apparent density of a Beulah coal ash sample (composition for different coal ashes used in this study are given in Appendix A) and the corresponding deposit sintering temperature. Three zones can be here distinguished: Zone 1, assigned to the formation of closed pores, and Zones 2 and 3, corresponding to pore-shrinkage and pore-filling by melt re-location, respectively. The minimum apparent density, which corresponds to the maximum volume of a sample (expressed by the volume of both ash particles and closed pores), occurs at the characteristic temperature of sintering, T_{cts}.

The characteristic temperature of sintering is here defined as the temperature at which the sintering mechanism changes from the formation of necks and pores into pore-shrinkage and pore-filling by melt. The T_{cts} gives information about the temperature until which the degree of sintering process is not pronounced; above this temperature a significant increase in both the sintering rate and the strength of the deposit will occur.

The characteristic temperatures of sintering for different coal ashes can be determined from the curves shown in Figure 5. Beulah coal ash has the lowest content of SiO_2, while Illinois No.6 and Pittsburgh No.8 coal ashes have approximately twice as much SiO_2. Beulah coal ash also has the highest content of CaO, MgO and Na_2O compared to the rest of the samples. These composition differences cause the low T_{cts} of Beulah and Montana subbituminous coal ash (700-800^{0}C), and the high T_{cts} of Illionis No.6 and Pittsburgh No.8 coal ashes.

1.2.1.2. Shrinkage

Shrinkage results from the change of shape of the samples: neck-shrinkage occurs mainly in the early stage of sintering, while shrinkage of closed pores and pore-filling (in the case of large excess of liquid phase) occurs at the later stages of sintering [15]. These processes depend on the liquid dynamics in capillary-like media, which may be deducted from physical properties of ash and ash species, such as viscosity, surface tension, and diffusivity.

Figure 6 shows the linear dependency of the compressive strength on the shrinkage. The shrinkage strain $(l_i - l_0) / l_0$, where the l_0 is the original diameter of the specimen, and $l_0 > l_i$. The

compressive strength of the sintered ash pellets was measured at room temperature. Two regions can be distinguished here: 1) the relatively low sample strength, when the sintering occurs in zone 1 (small amount of melt); and 2) significant increase in the sample strength, when the sintering takes place in zones 2 and (mostly) in zone 3. When a small amount of melt is present in a coal ash, the melt provides adhesion to substrates by the formation of necks, which correspond to zone 1 of the sintering. This leads to a local densification of a limited number of particles, which gives the deposit low deposit strength, and makes it suitable for removal by sootblowing (e.g. the sootblowing operation pressure for coal deposits: 9.0-14.0 MPa) [15]. In the case of a larger volume fraction of the liquid phase (zones 2 and 3), the sintering may result from shrinkage of the pores and viscous flow of the melt, which lead to a significant increase in strength.

1.2.1.3. Sintering Rates in Different Parts of a Boiler

Tran et al. [8] investigated the sintering characteristics of deposits in a kraft recovery boiler. In the kraft recovery boilers, schematically shown in Figure 7, black liquor is combusted in order to: 1) to regenerate sodium sulphide from sodium sulphate, contained in black liquor, 2) to generate steam, and 3) to eliminate undesired by-products, formed during cellulose production process. Black liquor is a recycled by-product of pulping of wood in the paper-making industry. According to Bernath et al. [17] the deposit formed during the combustion of black liquor almost entirely consists of salts Na_2CO_3 and Na_2SO_4. Unlike straw and coal ash deposits, the deposits from the kraft recovery boilers contain no silica and calcium.

According to Tran et al. [8], the deposits in the superheater region and partially in the boiler bank (colder regions of the boiler, where the combustion heat is transferred to the working fluid by convection) are dense and hard, so they can not be removed by brittle break-up. They showed that sintering, as a process of increasing the deposit density and strength, is particularly important in the boiler bank of the kraft recovery boiler, because here the flue gas temperature is in the range in which maximal sintering occurs.

This study provides the information about the deposit behaviour in different parts of the kraft recovery boiler:

- The flue gas temperature at the superheater inlet and outlet are typically 850-900^{0}C, and 550-650^{0}C, respectively. These temperatures enable considerable melting, sintering and grain growth within a kraft recovery ash deposit. The metal temperature in the lower superheater region (closer to the furnace region) is about 500^0, providing the conditions for the attached deposit layer to be rapidly sintered. The metal temperature in the higher superheater region (further from the furnace region) is usually lower than 450^{0}C, so the sintering of the attached deposit layer will be less pronounced, making the deposits easier to remove.
- The flue gas temperature at the entrance of the boiler bank is app. 600^{0}C, and app. 400^{0}C at its exit. The typical temperature of the tube surface is app. 320 ^{0}C, leading to slow sintering of the attached deposit layer. As the deposit thickens is increasing during the boiler operation, the deposit outer surface temperature increases. Sintering becomes more rapid, leading to increased hardness of the outer deposit layer. Such deposits can be removed from tubes by sootblowing, by breaking the weak bonding between the friable inner deposit layer and the tubes. Hard deposits may be formed in the boiler bank, if the local deposit temperature is at least 500^{0}C.

- The flue gas temperature at the entrance of the economizer section is typically 350-400^{0}C, and app. 250-300^{0}C at its outlet. These conditions usually do not lead to serious sintering or sootblowing problems.

1.2.2. Types of Deposit

The deposit characteristics depend on composition, the local environment (temperature, gas flow pattern, velocity) and the temperature of the heat transfer surface on which the deposit is formed. Miles et al. [18] show that alkalis in annual biomass fuels create serious fouling and slagging problems in conventional boilers.

Deposits, formed e.g. in PF-boilers can be divided into two major types:

- **Slagging deposits**, usually located in the radiant section of the boiler (high temperature region, directly exposure to radiation from the flame), are non-particulate, as a result of assimilation of particles into a liquid phase.
- **Fouling deposits**, formed in the convective pass of the boiler, usually contain a low level of molten phases.

1.2.2.1. Slagging

Slagging usually refers to deposits within the furnace, on areas that are directly exposed to the flame radiation, i.e. the hottest parts of the boiler, such as furnace walls, and in some cases widely spaced pendant superheaters. Miles et al. [18] investigated deposit formation during biomass combustion in grate fired units. They reported the presence of hard, fuse, glassy deposits in the furnace area and on the grate.

The surface temperature of the water walls in a coal fired pf-boiler are typically too low (200 - 400^{0}C) to cause melting of the initial deposit layer, which consists primarily of small, lightly sintered particles and few larger adhered and impacted particles [14,19]. As the deposit grows, its surface temperature increases, and eventually passes the melting temperature of the low temperature melting deposit material. The increase in the deposit surface temperature causes the softening and even melting of the deposit. In extreme cases deposit slag may run down the water walls. Due to the existence of melt, most of the fly ash particles that reach the surface tend to stick to it, causing the outer deposit layer to have a composition similar to the bulk fly ash composition.

Some boilers, so-called slag-trap furnaces, are designed to have ash removal by slagging. In other cases slagging deposits affect the over-all boiler efficiency, by reducing the heat transfer due to changes in the radiative properties and the thermal conductivity of the system. In these cases, for the satisfactory boiler operation long term build-up of slag deposits should be avoided.

1.2.2.2. Fouling

Fouling process refers to deposits in the areas that are not directly exposed to thermal radiation, such as more closely spaced tubes in the convection sections of a boiler. They consist of fly ash particles and condensed volatile species and are loosely bonded. For coal, fouling is divided into two regimes: high temperature fouling and low temperature fouling [20,21]. The particle-to-particle bonding mechanism in these two types of fouling differs. High temperature fouling occurs in regions where temperatures exceed the stability of the sulphate phases, i.e. above approximately 1050°C in coal fired boilers [21], and consists of fly ash particles which

are primarily bonded together by silicate phases. In the low-temperature fouling bonding is obtained through formation of sulphate phases [13,21].

1.3. Deposit Composition and Structure in Straw-fired Boilers

Due to the difference in composition, ashes formed during coal and biomass combustion behave differently. The composition of biomass-derived ashes also differs significantly because of the wide range of biomasses used.

The difference in the typical composition between a bituminous coal ash and a cereal straw ash is provided in Table 1. The table shows that the major constituents in the straw ash are silica, potassium, chlorine, calcium and magnesium. Compared to coal ashes, biomass ashes contain larger amounts of chlorine, but smaller amounts of sulphur, aluminium and iron. The significance of the high content of inorganic volatiles, i.e. chlorine and potassium, in biomass ashes is very important for both fly ash formation and ash transport mechanisms.

According to Nielsen [20], the large quantities of volatile inorganic species imply that the condensation of vapours, both as submicron particles (homogeneous condensation) and on the surface of ash particles, are more pronounced in biomass-fired boilers than in coal boilers.

According to Andersen [13], alkali sulphates dominate the composition of the inner layers of hotter deposits, while sulphates and chlorides are major components in deposits collected at colder sampling points. Chlorine salts, present in biomass ashes, are the major cause for severe corrosion of the superheater tubes.

The presence of alkali elements also influences the deposit characteristics, e.g. melting behaviour, which is important for the ash deposit build-up and shedding. Potassium forms low melting compounds with silicon, meaning that the overall melting range of a biomass ash is significantly lowered [3]. This is why biomass ash partly melts during thermal conversion and increases the sticking tendency to heat transfer surfaces.

Jensen et al. [3] reported deposition probe studies from two grate-fired boilers (Haslev and Slagelse CHPs, Denmark), burning eight types of cereal straw. The superheater deposits had a composition very similar to the fly ash, whereas the furnace deposits were enriched in silicon and calcium. The chemical analysis of mature deposits from a grate-fired boiler (Masnedø, Denmark) burning straw, done by Hansen et al. [22], showed that the inner part of the deposit contains high amounts of chlorine and potassium, and only small amount of silicon; the middle part is highly dominated by potassium and chlorine, but increasing amounts silicon and calcium is observed; the outer part contains almost no chlorine, but consists mainly of potassium, calcium and silicon. All the deposits had a characteristics layered structure, with a dense K_2SO_4 layer present next to the metal surface, as shown in Figure 8. The sulphation was noticed mainly in the Masnedø boiler [22], in contrast to the other straw-fired boilers examined (Haslev, Slagelse [1]), probably due to the relatively high steam temperatures at this plant (~560^{0}C). A physical description of the layers is given in Table 2.

The presence of a K_2SO_4-layer was explained [22] by initial deposition of KCl on the superheaters, and its subsequent sulphation. This is supported by the thermodynamic equilibrium calculations, shown in Figure 9, and by the fact that deposition probes, which were inserted in the boiler for some hours, did not contain K_2SO_4. Based on the calculations presented in Figure 9, done by Nielsen [20], solid phase K_2SO_4 and KCl are predicted to be thermodynamically stable at the metal surface temperature (~560^{0}C), i.e. around this temperature they are likely to be present in the condensed phase. In the matching flue gas, with the higher prevailing temperature (1000-1150^{0}C), the thermodynamically stable species are gaseous KCl, and small fractions of gaseous KOH and K_2SO_4. Since the condensed K_2SO_4 is

more stable at higher temperatures than condensed KCl, this indicates that KCl would not condense on top of the K_2SO_4 layer (since the surface temperature of the subsequent layer is higher), as might be indicated from the deposit structure. The conclusion is that KCl is the initially deposited species, which later reacts with a sulphur-containing species (most likely SO_2 or SO_3) to form the inner layer of K_2SO_4.

2. Shedding of Ash Deposits

Fireside deposits, formed on heat transfer surfaces, can drastically reduce the boiler thermal performance and, in severe cases, completely plug the flue gas passages and lead to unscheduled and often very costly boiler shutdowns. Effective deposit removal is therefore critically important in order to ensure maximum boiler thermal efficiency.

Shedding is a process of deposit removal, when pieces of the deposit separate from the tube, and drop off. Deposits can be removed, i.e. shedded, naturally without any operational influence, or shedding can be artificially initiated using, e.g. sootblowing or load changes. In industrial boilers, devices for ash deposit removal are usually implemented into the boiler construction. Techniques for tube cleaning, implemented in the boiler operation, are practical as long as ash deposits are not highly sintered or strongly attached to the surface. The knowledge about deposit growth and development is thus very important, and can be used for optimising the shedding process.

Shedding is directly affected by the strength development in the deposit. Principally, deposits gain strength by two processes: 1) solidification of molten or partially molten material, and 2) sintering of solid particles. Solidification is dominant in the regions with the high flue gas temperature, such as the superheater region. Sintering is dominant in the lower temperature regions, such as boiler bank and economizer inlet [7].

2.1. Mechanisms of Deposit Removal

Ash deposits can be removed from boiler heat transfer surfaces using artificially caused methods, e.g. by sootblowers, but deposit can also be removed without any external influence. Spontaneous shedding can be caused by: erosion, gravity force and thermal tensions. Artificial shedding is caused by operationally induced erosion, and mechanically and thermally induced stresses in the deposit. In this case, following mechanisms can be involved: break up due to high internal stresses, debonding from the tube surface, removal due to tube bending or vibration and thermal shock.

The shedding mechanisms can be classified in two ways:

- Based on the part of the deposit where shedding takes place, as given in Table 3.
- Based on the deposit type, as given in Table 4 (modified from [23])

As presented in Table 3, it is assumed that the locations where the removal of deposit material occurs are the deposit surface, the deposit tube-interface, and inside the deposit mass. Erosion and melting are causing the removal of the deposit mass from the deposit surface. On the other hand, gravity force, mechanically and thermally induced stresses cause removal of the deposit mass from the tube surface or they cause break inside the deposit itself.

Table 4 shows how different shedding mechanisms influence different deposit types. While erosion and gravity force can cause shedding of powdery deposits, they do not influence heavily sintered deposits and running slags. Running slags are removed from the heat transfer surfaces by melting. Heavily sintered deposits are shedded mainly due to thermal stress, and, to

a lesser extent, due to mechanical stresses [23]. Mechanical stresses mainly influence shedding of powdery and lightly sintered deposits.

2.1.1. Nature of an Ash Deposit

Which mechanism that will be dominant in different parts of the boiler depends among other properties on the characteristics of the deposited material. Two main types of deposits can be distinct: 1) ductile (plastic) deposits, and 2) brittle deposits. The difference between the ductile and the brittle deposits and their failure is shown in Figure 10.

Piroozmand et al. [7] investigated behaviour of deposits in the kraft recovery boilers, by using precipitator dusts, consisting mainly of sulphate and carbonate salts (compositions of investigated precipitator dusts are given in Appendix A). The investigation showed that the chloride content will influence the transition temperature between brittle and ductile deposits. For deposits that contain no chloride, the brittle-to-plastic transition occurs at high temperatures (around 700^0C), that are correlated (but usually lower), than their first melting temperature (FMT). The FMT is defined as the temperature at which the first melt appears in the deposit. When deposits contain chloride, they are brittle at temperatures up to 500 – 550^0C, and become ductile at higher temperatures. The transition temperature is close to the deposit FMT. The ductile-to-plastic transition is shown in Figure 11, as a sudden decrease of the deposit bend strength above a certain temperature. It should be noted that samples A, B, C and D contain chloride, and E sample does not.

For deposits which contain some chloride, as are deposits from the kraft recovery boilers, it can be expected that they will be brittle at temperatures up to their FMT. For a typical recovery boiler deposits, FMT usually varies from 510^0C to 600^0C, depending up on the potassium and carbonate content. Thus, these deposits are brittle in the colder boiler regions (e.g. downstream of the boiler bank inlet); in the superheater region (the flue gas temperature in the range 600^0C to 850^0C) deposits are plastic (or fluid) on the outer surface, but are brittle near the tube, where the temperature is lower than FMT [7].

The properties of brittle deposits from kraft recovery boilers, such as compressive, bending, and tensile strength were studied by Ebrahimi-Sabet [24]. In the experiments, gypsum was used to simulate brittle deposits. Its physical properties, such as fracture strength (the normal stress at the beginning of fracture) and porosity, were varied by changing the plaster-to-water ratio before casting.

2.1.2. Erosion (A)

Deposits are eroded away as non-sticky fly ash particles (mainly quartz) collide with non-sticky areas on the deposit surface, as shown in Figure 12. Erosion damage may be described as the gradual removal of material caused by repeated deformation (resulting from the normal component of the incoming particle impact velocity) and cutting actions (related to the tangential component of impact velocity) [25]. The deformation wear is more prominent for the brittle materials, whereas ductile materials are eroded mainly by the cutting mechanism.

Sootblowing can also causes erosion of the deposit, especially when saturated stream is used as the sootblowing medium. Water may condense out of saturated stream, creating small water droplets in the sootblowing jet. These droplets can impact the deposit and erode it.

In the case of pulverized-coal fired boilers, erosion wear damage usually occurs in the low-temperature regions, e.g. (primary) superheaters and reheaters, and in the water preheaters (economizers) [26].

2.1.2.1. Influence of the Deposit Characteristics

The study of Latella et al. [27], which deals with the erosive wear susceptibility of porous and nearly-fully-dense liquid-phase-sintered alumina ceramics, showed that the sample porosity influences both its mechanical properties and the erosion performance. Experiments showed that in a low porosity sample (2.5 %), the erosion removal occurred mainly by intergranular cracking and chipping. Mass removal due to erosion was higher when the sample of higher porosity (17.8 %) was tested, for all the impact angles. This is due to a plastic cutting mechanism, particularly at low impact angles, in association with a brittle fracture. A relatively low material hardness of the highly porous structure (17.8 %) is likely to contribute to a significant enhancement in inelastic deformability, due to highly localized stresses from impacts, which will contribute to extensive material loss. Thus, the material of higher porosity is more susceptible not only to inelastic deformation, but also to exaggerated erosive wear.

According to Oka et el. [28], it is generally considered that the material hardness is one of the main mechanical property associated with erosion damage. Beside hardness, the elastic modulus and the yield strength are thought to affect erosion damage, sometimes with the mixed effects of these properties. Brittleness seems to be useful in characterizing erosion of ceramic materials. An erosion-wear-resistant material has a hardness value higher than that of the impacting-particle material. Results presented by Raask [26] indicate that a wear resistant material should have a hardness value about 500 kg/mm^2 higher than that of the impacting particles. The hardest mineral species in coal and biomass fly ash is quartz [26], having the hardness value of about 1100 kg/mm^2. For the tube erosion [27], the usual indication for an abrasive ash is high silicate content, and a high ratio of silicate to alumina.

Heat treatment has different effects on hardness of different minerals [26]: for soft minerals (e.g. kaolin, illite, muscovite) the hardness is increased (T = 1500 - 1700 K, H = 100 - 500 kg/mm^2); for hard minerals (e.g. pyrite and quartz) the hardness is reduced on heating, either completely (pyrite), or partially (quartz).

The impact angle, α, which is defined as the angle between the material which is to be eroded, and the trajectory of the erodent particles, has an important role for erosion [29]. It depends on the nature of the impacted surface. The maximum erosion rate of ductile materials (e.g. metals and alloys) is at the intermediate impact angles (e.g. 15^0, 30^0). The maximum erosion rate of brittle materials (e.g. glass) is usually at the normal impact angle (90^0).

2.1.2.2. Influence of the Incoming Particle Characteristics

According to Raask [25], erosion rate is influenced by the shape of the incoming particles. Highly abrasive, hard, and angular quartz grains cause erosion by cutting, whereas glass spheres produce a surface deformation first, leading subsequently to a brittle failure. The non-abrasive aluminosilicate particles vitrify and agglomerate in the boiler flame. The ash emerging from a high-temperature flame largely consists of spherical particles. Surface characteristics of typical aluminosilicate and quartz particles are shown in Figure 13.

A study of Sundararajan and Roy [30] showed that the erosion rate is independent of the particle hardness if the erodent particles are at least twice as hard as the target material. When the hardness of impacting particles, H_p is less than that of the eroded material, H_m, the wear rate is inversely proportional to the hardness difference (H_m-H_p). The erosion rate is significantly lower if the hardness of the erodent particles is comparable to that of the target material.

Erosion wear is also influenced by the particle size of the impacting material. For the quartz sand as an erodent, the rate of erosion is insignificant when the diameter of the

impacting particles is below 5 μm [26]. Small particles have a small amount of the inertial momentum, and they are carried around the object by the gas flow. For the fly ash particles larger than 45 μm the erosion rate is found to be constant.

2.1.2.3. Influence of Impact Velocity

The impact velocity influences the erosion wear of a material by increasing the amount of eroded mass. The erosion wear, E [mm^3/kg], which is defined as the rate of material loss from the eroded target per unit weight of impacting material, is expected to follow a power low [25]:

$$E = a \cdot v^n \tag{4}$$

where a is the erosion wear coefficient, influenced by the properties of the impacting particles, the target material and the impaction angle, and n is the velocity power index. This equation suggests that erosion damage is basically proportional to the impact energy [31].

According to Oka et al. [32] , the equation for the erosion wear at a normal impact angle, E_{90} can be expanded as:

$$E_{90} = K \cdot (H_v)^{k_1} \cdot (v)^{k_2} \cdot (d)^{k_3} \tag{5}$$

where k_1, k_2 and k_3 are the exponent factors, K is the particle property factor, which includes the particle shape (angularity) and the particle hardness, and d is the particle diameter.

Data presented in [26] show that n for fly ash (d = 75-105 μm), when impacting austenitic steel with velocity 90-300 m/s, is 1.2 - 1.4. The same source gives an equation for the erosion wear of soft materials, (aluminium and copper), where the impact velocity is raised to the power of 2.4.

2.1.2.4. Erosion Modeling

Modeling of the deposit erosion phenomenon is not widely discussed in the open literature, although a similar phenomenon, i.e. erosion of boiler tubes by impacting particles, has been studied more thoroughly [25,26]. The main problem with the existing tube-erosion models is their inability to account for the formation of an ash deposit on the tube surface. Also, important parameters in these models are the hardness of both the particle and the surface materials, which are difficult to estimate for ash particles and an existing deposit surface.

Walsh et al. [12] developed a model, formulated in equ. (3), for calculating the net mass fraction of impacting particles that form a deposit, f_{dep}, i.e. the result of the simultaneous processes of sticking and erosion, occurring by collision of incoming particles with the particles on the deposit surface. The rate of erosion used in this model is assumed to be proportional to the flux of impacting particles, the mass fraction of incoming non-sticky particles, and the fraction of deposit surface area that is not sticky. The non-stickiness is important because the erosion is performed by the solid-solid material collision. The draw-back of this approach is the fact that the parameter k_e and the probabilities distribution have to be determined empirically.

Oka et al. [29,31,32] developed an erosion model, based on the idea that the erosion wear is the product of two factors; the first factor is related to the vertical component of the impact energy and approximates repeated plastic deformation, and the second factor indicates the approximately horizontal component related to the cutting action. It was assumed that the effective parameters for erosion damage are the impact velocity, the angle, the particle characteristics (size, shape, etc.), and the hardness of the target material. The erosion wear at arbitrary impact angles, $E(\alpha)$ [mm^3/kg] is expressed as:

$$E(\alpha) = g(\alpha) \cdot E_{90} \quad (6)$$

where E_{90} is the erosion wear at normal impact angle, and $g(\alpha)$ is the ratio of erosion damage at arbitrary angles, to that at normal angle, E_{90}. The impact angle dependence of normalized erosion, $g(\alpha)$ can be expressed by the two trigonometric functions and by the initial material hardness number, H_v [GPa] as:

$$g(\alpha) = (\sin\alpha)^{n_1} \cdot (1 + H_v \cdot (1 - \sin\alpha))^{n_2} \quad (7)$$

where n_1 and n_2 are exponents determined by the material hardness and the particle properties, including the particle shape. They are indicators of the deformation and the cutting actions, respectively. The first term in equ. (7) is associated with repeated plastic deformation, while the second term shows cutting action, which is relative and more effective at shallower impact angles. Function $g(\alpha)$, as a function of the two erosion mechanisms, i.e. deformation and cutting, is shown in Figure 14.

2.1.3. Gravity Shedding and Flow of Liquid Slag (B, C)

Gravity shedding is caused by the gravity force (deposit weight), which acts on the deposit and tends to break it down. The force balance is established between the gravity force and the forces which keep the deposit on the (tube) surface: 1) the adhesion strength (between the deposit and the tube), or 2) the deposit tensile strength (between/inside the deposit layers). When the gravity force is greater than the strength of the bond within the deposit (break-up of weak deposits) or between the deposit and the tube (detachment of deposit pieces), the deposit will fall off, as shown in Figure 15. Gravity shedding of ash deposits depends on the gas temperature distribution within the boiler (influencing the ductility of material), deposit composition and deposit sintering.

Another form of gravity shedding is deposit removal by melting. If the combustion conditions are suitable for the development of the low-viscosity slag deposits (e.g. due to a high flue gas temperature), molten deposit may run down the boiler walls. The temperature gradient through such a deposit will cause the slag layers close to the wall surface to be solid, while the outer deposit layer will be molten. With a relatively constant flue gas temperature, an equilibrium deposit thickness should be reached, where the mass flow of running slag balances the mass flow of depositing particles. Experimental investigation of ash deposition and removal in a biomass fired boiler [33], showed that melting is an important deposit shedding mechanism.

Provided that the composition of the deposit is known, the fraction of melt in a deposit can be found using experimentally determined melting curves [14]. Melting curves depend strongly on the deposit composition, like the ratio of potassium salts to silicates. A larger fraction of silicates would reduce the melt fraction correspondingly, which is observed from the melting curves of the furnace deposit and the bottom ash.

A simple mathematical description of a thick film flow down a plane, vertical surface, with uniaxially varying composition and temperature, was developed by Vargas [34]. A melt layer of constant thickness, D is divided into N sub-layers ($1 \le n \le N$) of constant composition and temperature, i.e. constant viscosity, μ_n and density, ρ_n. As is the case for most condensed phases, the densities of silicate melts of constant composition are almost independent of the temperature, in which case the model simplifies to:

$$v - v_n = \frac{\rho \cdot g}{2 \cdot \mu_n} \cdot (x_n^2 - x^2) \qquad (8)$$
$$x \in [x_{n-1}, x_n], \quad x_N = D, \quad v_N = 0$$

where x is the distance from the deposit surface, v is the linear flow velocity, and g is the gravitational acceleration. Model is schematically presented in Figure 16.

Kaer [35] numerically modeled heat transfer through an annular deposit formed on a superheater tube, taking into account the variation of heat transfer properties during deposit growth. Using this model, the flow of a slag down a vertical section of a superheater tube was further predicted. In the steady state, the mass flow rate of depositing particles is balanced by the removal caused by the flow of a running slag. Figure 17 shows the mass fluxes considered by the model. The running slag is assumed to start at the upper end of the tube,

Conservation of mass. Considering the solid deposit layer, which consists of cylindrical shells of fixed inner radius and a moving outer boundary, the change of mass due to solidification at the inner boundary is zero. The mass flux across the outer boundary may either be due to particles deposition, or due to liquefaction/solidification of the succeeding layer. The time rate of change of the solid deposit outer radius is calculated as [35,36]:

$$\frac{dR_s}{dt} = \begin{cases} \dfrac{m_{dep}''}{\rho_s \cdot (1-p)}, & R_l = 0 \\ \dfrac{m_{sol}''}{\rho_s \cdot (1-p)}, & R_l > 0 \quad and \quad m_{sol}'' < \\ \dfrac{m_{sol}''}{\rho_s}, & R_l > 0 \quad and \quad m_{sol}'' > \end{cases} \qquad (9)$$

where R_s [m] is the outer radius of the solid deposit, R_l [m] is the outer radius of the liquid deposit, m_{dep}'' [kg/m^{2}s] is the deposition flux of particles, ρ_s [kg/m^3] is the density of the solid phase, p is the deposit porosity, and m_{sol}'' [kg/m^{2}s] is the liquefaction/solidification flux.

When no liquid phase is present, i.e. $R_l = 0$, the rate of change of the solid radius equals to the ratio of the deposit mass flux and the bulk gas density, ($\rho_s \cdot (1\text{-}p)$). When the melting temperature is reached, a liquid layer is formed, and the rate of change of the solid radius is given by the mass flux of material melting or solidifying.

For a liquid slag layer, the inlet and the outlet mass flux, due to the slag flow, has to be accounted for, in order to obtain the time change of the liquid outer radius:

$$\frac{dR_l}{dt} = \frac{\left(m_{dep}'' + m_{sol}''\right) + m_{flow,in}'' - m_{flow,out}''}{\rho_l} \qquad (10)$$

where $m_{flow,in}''$ [kg/m^{2}s] is the mass flux of liquid flowing into the control volume, $m_{flow,out}''$ [kg/m^{2}s] is the mass flux of liquid flowing out of the control volume, and ρ_l [kg/m^3] is the liquid density.

Conservation of momentum. Assuming that the flow of the liquid layer is laminar, the one-dimensional momentum equation for a Newtonian fluid is:

$$\frac{1}{r}\frac{d}{dr}\left[\mu r \cdot \frac{du}{dr}\right] = -\rho g \tag{11}$$

where μ_l [Pas] is the liquid viscosity, and g [m/s^2] is the gravitational acceleration. The velocity profile is then expressed as [35]:

$$u(r) = \frac{\rho}{4}\cdot\frac{g}{\mu}\cdot\left[2\cdot R_l^{\,2}\ln\left(\frac{r}{R_s}\right) + \left(R_s^{\,2} - r^2\right)\right] \tag{12}$$

The mass flux of the running slag can be found by integration of the velocity profile:

$$m_{slag}'' = \frac{\pi\cdot\rho^2\cdot g}{8\cdot\mu}\cdot\left[4\cdot R_l^{\,2}\ln\left(\frac{R_l}{R_s}\right) - 3\cdot R_l^{\,4} + 4\cdot\left(R_s\cdot R_l\right)^2 - R_s^{\,4}\right] \tag{13}$$

Conservation of energy. Assuming that the axial temperature gradient is small compared to the radial temperature gradient, the heat transfer can be modeled using the one-dimensional energy equation, in cylindrical coordinates:

$$\frac{d}{dr}\left(k\,r\cdot\frac{dT}{dr}\right) = S \tag{14}$$

where k [W/mK] is the deposit thermal conductivity, and S [W/m^2] is a source term. The source term is zero everywhere except at the nodes, where liquefaction or solidification occurs.

The obtained thicknesses of the solid and the liquid layers in the steady state are shown in Figure 18. The location of the interface between the solid and the liquid layers is governed by several factors. As the deposit is evolving in time, the existence of a liquid layer on top of the solid layer reduces the local temperature inside the deposit, due to insulating effect. As the thickness of the liquid layer increases, part of the liquid layer, attached to the solid surface, solidifies, due to the temperature decrease below the deposit melting temperature (m_{sol}'' in Figure 17). Solidification of the liquid material is the most pronounced during the initial formation of the liquid layer, i.e. when the vertical location tends to zero. This is caused by the rapid increase of the liquid layer thickness, and a correspondingly strong insulating effect, which is presented in Figure 18 by the steep increase of the surface temperature. If the heat flux between the flue gases and the surface of the running slag is much higher compared to the heat flux between the deposit and the working fluid, melting of the solid deposit may occur (m_{liq}'' in Figure 17).

The model results are influenced by the deposition flux and the slag viscosity. Thus the heat transfer prediction and the flow of the running slag should be considered as a qualitative indication of the potential effects of a deposit on heat transfer rates.

2.1.4. Thermal Shock (D)

Thermal stress occurs due to an uneven thermal expansion (thermal mismatch) between the deposit and the tube metal, or between different deposit layers. The thermal expansion is directly influenced by the thermal expansion coefficient, α [m/mK], which is defined as the increase in the length of a sample, per unit increase in temperature. The thermal expansion coefficient determines if the materials are thermally compatible. Also, sudden heating/cooling may cause thermal shock of the material. The sudden shrinking of a deposit caused e.g. by a

sudden cooling, decreases the adhesion force between a deposit and a tube. Thermal stresses may lead to deposit crack, as shown in Figure 19.

Different sootblowing mediums are used for deposit removal. Water is the most effective medium for removing heavily sintered or slagged deposits. Sootblowing can also cause thermal shock, if the temperature difference between the sootblowing medium and the deposit is large enough to cause significant deposit shrinking. Additionally, the use of water creates a pressure wave, due to a quick expansion of liquid water to steam.

2.1.4.1. Thermal Compatibility of Ash Deposits and Boiler-Tube Surfaces

Thermal compatibility between materials can be obtained by comparing their thermal expansion coefficients. The experience from the fabrication of glass/metal seals and manufacturing of enamel-coated products [25,37] show that for strong seals or adhering coatings, it is necessary to have compatible coefficients of the thermal expansion for metal, α_m and coating material, α_g. For an enamel coating on steel [25,38] it is appropriate to have $\alpha_g \cong 0{,}9\ \alpha_m$. This is because steel is strong in compression as well as in tension, whereas glass is strong in compression, but weak in tension. On cooling, the glass phase of a metal/glass seal will remain in compression, and a failure would not take place as long as the residual unbalanced stress does not exceed the interface bond strength. In case of adherence of ash deposits on boiler tubes, a certain difference between the thermal properties is important, and it will influence the adhesive bond on thermal cycling.

The thermal expansion coefficients of steels and deposit constituents are shown in Table 5. In the case of mild-steel, there is no gross incompatibility in the thermal expansion characteristics ($11\text{-}12 \cdot 10^{-6}\ K^{-1}$ for mild-steel, and $5\text{-}9 \cdot 10^{-6}\ K^{-1}$ for deposit constituents), and when strongly bonded ash deposit is once formed on a tube, it is not easily removed by thermal cycling. The thermal expansion of austenitic steel ($16\text{-}18 \cdot 10^{-6}\ K^{-1}$) is significantly higher than that of oxides and deposit materials. In the absence of a boiler deposit, the metal oxide material ($8\text{-}10 \cdot 10^{-6}\ K^{-1}$) in the form of a thin film is able to absorb thermal stresses, and the adhesive film remains intact on cooling. But it appears that the oxide layer is unable to absorb thermal stresses in a similar manner when contaminated and constrained by bonded ash deposits. It is therefore common that ash deposits peel-off austenitic tubes upon cooling, whereas the deposit formed on ferric steels under the same conditions, remain firmly attached to the tubes [25].

2.1.5. Brittle Break-up

A sootblower jet impact can cause high internal stresses in the deposit. For weak, brittle deposits this leads to a deposit break-up, as shown in Figure 20 (a). Brittle failure originates from the deposit surface, which is directly affected by the jet pressure. The jet penetrates into the flaws on the deposit surface and opens them, causing the deposit to break. According to [24], when a jet hits a brittle deposit, it shatters the deposit into pieces.

The analysis [24,39] showed that for a broad range of deposit geometries, deposit break-up depends only on the peak impact pressure, PIP (local stagnation pressure in a sootblower jet; further discussed in 2.1.6.1.), and the deposit tensile strength. The deposit tensile strength varies from location to location within a boiler, due to variations in the deposit composition, the formation mechanism and the flue gas temperature.

The criterion for deposit removal by brittle break-up was calculated in terms of PIP, by Jameel et al. [40] as:

$$PIP > \frac{2 \cdot \sigma_t}{\cos \theta} \tag{15}$$

where σ_t [MPa] is the tensile strength of the deposit, and θ is the angle between the jet axis and the axis perpendicular to the tube axis. This criterion will be further discussed in Chapter 4.1.3.

2.1.6. Debonding

Investigation of deposition in kraft recovery boilers [39] showed that the flue gas temperature in the superheater region is usually high enough to rise conditions for development of deposits that are hard, and cannot be broken and removed by the brittle break-up mechanism. They are usually dense and may have a melted surface, due to the high temperatures of the deposit surface and the flue gas. Since deposits in the superheater region can be at least partially removed by sootblowing, it implies that some other removal mechanism than brittle break-up is present.

Dense, hard deposits can be removed by debonding from the tube surface, as shown in Figure 20 (b). A deposit is removed by debonding when the generated stress (e.g. by sootblowing) exceeds the adhesion strength at the tube-deposit interface. If a strong deposit is weakly attached to a tube surface, it might be removed by debonding even with a weak jet.

Debonding mechanism is influenced by the adhesion strength of the deposit-tube interface [6]. Adhesive bonding between the deposit and the tube surface is decreased when a powdery fume or porous layer exists as the deposit layer closest to the tube. The chemical composition and the thermal characteristics of the oxide layer, formed on the boiler tubes, influences the strength of the adhesive bond between an oxide surface and an ash deposit. Apart from the thermal shock, caused by the thermal mismatch, vibrations can also promote debonding, by decreasing the tube-deposit adhesive bond.

Several types of deposit-sootblower jet interactions can cause debonding [6,24]: 1) jet impact direction induces a shear stress on the deposit-tube interface, 2) jet impact induces high frequency vibration in the deposit-tube system, and 3) large scale tube banding and flexure, caused by the impingement of the high velocity jet, may induce strains in the brittle deposits, leading to failure and debonding.

The ability of a sootblower jet to debond a deposit from a tube surface depends on many factors, including the jet characteristics, the bond strength at the deposit-tube interface, the size and the shape of the deposit, and the tube area, covered by the deposit [6,24]. The adhesion strengths of molten precipitator dusts (from a kraft recovery boiler) dripped onto a steel plate and heated to various temperatures characteristic for tube surfaces were experimentally obtained. Using the measured adhesion strength, and conclusions drawn from these experiments, the criterion for deposit removal by debonding was calculated as [6]:

$$PIP > \frac{1}{\psi_{max}} \cdot \sigma_{adh} \cdot \frac{d}{H} \tag{16}$$

where ψ_{max} is the maximum dimensionless tensile stress at the tube-deposit interface (it will be further discussed in Chapter 2.2.1.), σ_t [MPa] is the adhesion strength of the deposit, d [m] is the tube diameter, and H [m] is the deposit thickness.

Figure 21 shows the modeled PIP required for a deposit removal, as a function of a deposit thickness and the adhesion strengths, for two mechanisms of deposit removal, i.e. brittle break-up (equ. (15)) and debonding (equ. (16)). The rapid decline of required PIP with the increasing deposit thickness indicates that debonding is likely to be much more effective than brittle break-up for thick deposits.

2.1.6.1. Deposit Blow-off Experiments

Ebrahimi-Sabet [24] investigated the process of deposit debonding by a fluid jet impact. Wood was used to represent a deposit, since the tested material should not be fractured by the fluid jet. Gypsum was used as interfacial bonding material, because its strength can be measured and it could be altered easily by changing the water-to-plaster ratio. Two deposit shapes, were examined, as showed in Figure 22: flat and elongated - type A, and short and rounded - type B. To ensure that the model deposit would be debonded from the tube, at the bonding interface in the gypsum layer, a layer of carpenter glue was placed between the tube and gypsum, and gypsum and wood. Since the glue is a stronger bonding material than gypsum, debonding would occur in the gypsum layer.

Figure 23 shows the results obtained for the deposit type A. It can be noticed that a higher PIP is required to debond the deposit from the tube surface when the adhesion strength of the interface is higher. Similar results were obtained for both investigated deposit types, thus it was concluded that the deposit shape does not influence the debonding process.

2.1.6.2. Debonding Due to Vibrations

The sootblower jets and the flow of the flue gases may cause vibrations of boiler tubes and deposits. While excessive vibrations may lead to metal fatigue and ultimately to tube failure, moderate vibrations may break the bond between a tube and a deposit, thus being useful in deposit removal.

2.2. Determination of Stresses in the Deposit

Mechanical and thermal stresses, which may cause deposit failure, will be outlined and discussed in this section. Physical properties of the deposits that are relevant for the stress analysis are described in Chapter 3.

2.2.1. Mechanical Stresses

Although the distribution of stresses at a tube-deposit interface, when the deposit exact shape, material properties and the applied forces are known, can be calculated using the theory of elasticity, this approach is not recommended because [6]:

- The deposit shape can be characterized only approximately.
- The deposit mechanical properties are not uniform throughout the bulk of the deposit, because of the variations in the deposit porosity, temperature distribution and chemical composition. The outer layers are exposed to higher temperatures than the inner layers, and are more sintered and thereby harder.
- The aerodynamic impact of a turbulent sootblower jet on a deposit cannot be determined precisely, in terms of exact pressure distribution on the deposit surface of an arbitrary shape.

In order to estimate the stresses generated in the adhesion layer by a sootblower jet, a simplified theoretical model of deposit mechanical structure was developed by Kaliazine et al. [6]. The considered deposit-tube geometry is shown in Figure 24. The only input data needed

are the tube area covered with a deposit, and the applied net force. The maximum stress, σ_{max} at the tube-deposit interface, is a function of the two dimensionless parameters, α_0 and M/FR:

$$\sigma_{max} = \frac{F}{LR} \cdot \psi_{max}(\alpha_0, M/FR) \tag{17}$$

where $2\alpha_o$ is the angle of the tube covered with deposit, R is the tube radius, L is the deposit length, F is the net force of the sootblower jet, applied to the deposit in the transverse direction, M is the net moment of force around the axis of the tube, and ψ_{max} is the maximum dimensionless tensile stress at the tube-deposit interface, which is a function of the angle α_o, and the factor M/FR.

If the lateral force, F is known, the momentum, M can be approximately estimated from the deposit thickness, H as [6]:

$$M = F(R + H/2) \tag{18}$$

Equs. (17) and (18) indicate that a greater momentum induces greater stresses at the tube-deposit interface. The deposit removal becomes easier when the covered area of the tube is reduced (proportional to α_o) or the deposit thickness is increased, which is taken into account when parameter ψ_{max} was calculated. Value of the parameter ψ_{max} is in the range 0.7 to 1 [6], if the deposit covers half or more of the tube circumference, as shown in Figure 25. The detail formulation of interface stresses is presented in [41].

The parameter M/FR depends on the deposit thickness:

- For a thin deposit layer, the parameter M/FR ~ 1, since M = F·R. In this case, most of the deposit is located at the distance R from the tube axis.
- For thicker deposits, the same force causes a larger moment of force, and this parameter becomes larger, i.e. M/FR > 1.

Figure 25 shows the maximum dimensionless tensile stress at the tube-deposit interface as a function of covered tube angle. Parameter M/FR equals 1 in the case of a thin deposit, and M/FR equals 2 for a relatively thick deposit, i.e. with a thickness compatible to the tube diameter.

2.2.2. Thermal Stresses

Sudden change in the surface temperature of a material causes thermal stress, which may subsequently cause crack propagation. Thermal stress, caused by an instantaneous surface temperature change, ΔT and subsequent expansion and/or contraction, and the local stress can be calculated as:

$$\sigma = \frac{E \cdot \alpha \cdot \Delta T}{(1-\nu)} \tag{19}$$

where σ [N/m^2] is the stress caused by the temperature change, E [Pa] is the elastic modulus, α [1/K] is the thermal expansion coefficient, ΔT [K] is the temperature change, and ν [-] is the Poisson's ratio.

In practice the heat transfer rate is not infinite and the heat transfer coefficient, h [W/K m^2] also controls the thermal stress development [42]. Therefore, the equation (19) can be modified to include the conditions of heat transfer and conduction through the Biot's number, $\beta = h \cdot l/k$:

$$\sigma = \frac{E \cdot \alpha \cdot \Delta T}{(1-\nu)} \cdot f(\beta) \tag{20}$$

where l [m] is the characteristic dimension, and k [W/mK] is the thermal conductivity. According to [42], for slow cooling the Biot's number is less than one, and f (□) ≈ □

2.2.2.1. Thermal Shock Parameters

The thermal shock takes place when thermal stress reaches critical fracture stress, □$_{cf}$. According to equ. (19), the only variable which can cause an increase of stress is the change of surface temperature, □T. So, the critical stress will be reached when □T□□T$_c$.

Hasselman [43-47] formulated five thermal shock resistance parameters in order to describe the thermal shock behaviour of ceramics, in terms of their physical and mechanical properties. The thermal shock parameter R [°] is obtained by rearranging equ. (19), and it equals the critical temperature difference, ΔT imposed on the surface of a material under infinite heat transfer conditions, at which the tensile stress, σ, equals the fracture strength, σ_{cf} :

$$R = \sigma_{cf} \cdot \frac{(1-\nu)}{\alpha \cdot E} \tag{21}$$

Under finite heat transfer conditions, the thermal shock parameter is defined rather as □T$_c$= R$_{TS}$ ' = k R$_{TS}$, including thermal conductivity effect on thermal shock:

$$R' = \sigma_{cf} \cdot \frac{(1-\nu)}{\alpha \cdot E} \cdot k \tag{22}$$

According to Wain et al. [5], low values of R and R' indicate that a small temperature change would cause high thermal stress in the deposit, thus making it easily removable by sootblowing. High values of R and R' indicate high ΔT requirement to initiate crack propagation, i.e. the establishment of steep temperature gradients to produce critical thermal stress formation.

The thermal shock parameters R and R' are determined by both the thermal and the mechanical properties of the deposit. These properties depend on the deposit composition and the porosity. The longer the deposit remains on the furnace, the porosity will be often lower in the bulk deposit. As a result, the strength, and the thermal conductivity of the slag will increase, leading to an increase in the resistance of the slag to fracture by thermal stress, e.g. caused by the use of sootblowers. This suggests that frequent use of sootblowers is preferred, if deposits are to be removed without too much difficulty [5].

The variation of the thermal shock parameters R and R' for coal ash slags of different composition with respect to porosity, shown in Figure 26, is calculated by Wain et al. [5]. The calculation is based on the relationships that link thermal and mechanical properties of the deposit with porosity. It was assumed that the coefficient of thermal expansion and the Poisson's ratio are independent of porosity. The composition and characteristics of the coal slags, used in this study, is given in Appendix A.

The results in Figure 26 show that R-value decreases with the increasing porosity. For some slags R-value decreases more rapid than for others, although no simple relationship between the thermal shock coefficient and the composition of coal slags can be detected. Results indicate that the elastic modulus decreases more rapidly than the compressive strength, as the porosity increases. Practically, results presented in Figure 26 suggest that the resistance to fracture of coal slags, caused by thermal stresses, increases when the porosity is less than 25 % (v/v).

The values of R and R' should not be taken as absolute values, since the calculations have been made using the compressive strength, rather than tensile strength. Brittle materials, such as slags, are always stronger in compression than in tension, since surface flaws and microcracks do not influence compressive strength measurements.

3. Physical Properties of the Deposit

Both ash deposit formation rate and deposit properties are important parameters for the operation of a boiler. According to Salmenoya [10], important deposit properties for a successful operation of the biofuel-fired boiler include: (1) the ease of removal from heat transfer surfaces, (2) the effective thermal conductivity, (3) the physical strength, (4) the elemental and chemical composition, (5) the morphology and the porosity, and (7) the deposit melting behaviour.

Physical properties of solid deposits, relevant to the deposit build-up and removal process, are: the mechanical strength, the elastic (Young) modulus, the Poisson's ratio, the viscosity, the thermal conductivity, the thermal expansion coefficient and the melting behaviour. These properties are influenced by the deposit thickness, porosity and the deposit chemical composition.

3.1. Deposit Strength

The deposit strength is one of the major factors influencing the process of deposit removal, both naturally (spontaneously) and artificially (deliberately) induced. Studies [6,7,39] showed that the strength of the kraft recovery deposits is strongly related to the deposit porosity, its composition, and the temperature distribution inside it, as well as the temperature of the boundary interfaces (interface between a tube surface and a deposit, and interface between deposit layers). The dependency of the strength of different coal ash slags on porosity was investigated in [5].

3.1.1. Deposit Tensile Strength

The mechanical strengths, which are important for deposit removal, are the tensile and the bend strength, and the tube-deposit adhesion strength [7]. From a point-of-view of deposit removal, the tensile strength is the most relevant property, because the material tends to break at its weakest point.

The deposit properties, which influence the deposit tensile strength, vary from location to location within the boiler, because they depend on the deposit chemistry, the formation mechanism, the porosity and the flue gas temperature.

3.1.1.1. Influence of Porosity on Deposit Strength

Piroozmand et al. [7] experimentally investigated precipitator dusts from five recovery boilers (composition provided in Appendix A). They showed that the samples sinter and harden at different rates, depending on their particle size distribution, composition, and temperature. Experiments also showed that as the porosity of a sample starts to decrease (due to the increase in temperature), the bend strength of a deposit starts to increase, reaching the lowest value at the minimum porosity (for sample A, maximal strength is 15 MPa at porosity 0.13, at about 500°C). The bend strength suddenly decreases at temperatures above the first melting

temperature (530^{0}C for this sample), almost reaching zero at 600^{0}C. The low bend strengths of the pellet are presumably due to the presence of a liquid phase. It acts as a 'lubricant' between dust particles, causing the pellet to deform plastically rather than to break in a brittle manner.

In addition, the study of Kaliazine et al. [6] showed that the tensile strength of the sintered kraft recovery dust depends only on the sample porosity, as is shown in Figure 27.

The compressive strength of ceramic materials can be related to the compressive strength of a slag having zero porosity, using the relationship of Ryshkewitch [48]:

$$\sigma = \sigma_0 \cdot \exp^{-np} \tag{23}$$

where p is the porosity, and n is a curve fitting parameter. The experiments, which lead to this expression, were performed on sintered alumina.

According to Wain et al. [5], the data obtained for coal ash slags (composition and characteristics given in Appendix A) were found to fit this relationship. The values for σ_0 and n for a particular slag were obtained by plotting log σ against porosity, and by using a least-squares-fit to extrapolate to zero porosity and obtain the slope, n. Values for n varied from 4 to 25, and σ_0 was found to vary between 220 and 2780 MN/m^2. The compressive strength development for ten coal slags were calculated the using equ.(23), and the results are shown in Figure 28. In comments to [48], it is concluded that for sintered ceramic materials, like Al_2O_3 and ZrO_2, n is around 7. In study [7], dealing with the sintered precipitator dusts from the kraft recovery boiler, σ_0 is estimated to be 35 MPa, and n to be 6.2. It was also suggested that n can have values between 4 and 7.

The coal ash slags tested by Wain et el. [5] have a wide range of compressive strengths at zero porosity, with the greatest difference observed for the samples H and I. Sample H, which has the highest compressive strength, have the least weight fraction of silica oxide comparing to other samples, but the highest concentration of iron oxide. According to Figure 28, each coal slag sample shows a rapid decrease in strength as the porosity increases. The change is most marked in the range from 0 to 25 % (v/v); thereafter all the slags show similar low values for the compressive strength. For slags that have high initial porosity (as H in the Figure 28), extrapolation to zero porosity may cause large errors.

3.1.1.2. Influence of Temperature on Deposit Strength

It can be expected that the strength of boiler deposits is lower when measured at high temperatures, than at room temperature. Piroozmand et al. [7] measured bend strengths of sintered precipitator dusts from a recovery boiler both at room and at sintering temperature. Figure 29 shows the strength of the sample A, when measured at 400-550^{0}C, are 50% to 80% of the values measured at room temperature.

3.1.2. Deposit Adhesion Strength

Adhesion forces between two bodies may be characterized by the minimum shear or tensile stress, at the contact surface, required to cause separation. The higher the adhesion strength, the more difficult it is to detach a piece of the deposit from the tube surface. Adhesion forces depend on the tube surface conditions (temperature and roughness), the deposit particle size, and the deposit composition [6].

Kaliazine et al. [6] measured the influence of temperature on the deposit adhesion strength. Molten precipitator dust from the kraft recovery boiler was dripped onto a steel plate, and heated to various temperatures, characteristic for tube surfaces. The force required to remove the sample from the substrate was measured by a tensile strength machine, and the adhesion strength was then calculated. The results are shown in Figure 30. Based on these experimental results the following was concluded:

- The adhesion strength depends strongly on the substrate temperature. At low temperatures, the adhesion strength is low. With an increase in temperature, it increases to a maximum, and then decreases, probably due to the formation of a liquid phase.
- The adhesion strength depends on the sample size: it is greater for smaller samples, which is probably due to greater effect of thermal shock in the solidification of larger samples, or because larger samples have more and larger flaws, which may initiate failure.
- At temperatures above 450°C the adhesion strength between a deposit and a tube surface is much smaller compared to the tensile strength of a sintered dust. This implies that debonding is probably the dominant mechanism of removal in locations where sintering occurs.

Experiments [6] showed that the ratio between the adhesion strengths of the strongest and the weakest samples of molten precipitator dusts, coming from the kraft recovery boiler, was as large as 10. This indicates that even if the sootblower pressure is high enough to remove a portion of a deposit having the average adhesion strength, it may not be powerful enough to remove all pieces of the deposit from a given location. Removal of all pieces of deposit typically requires a Peak Impact Pressure (PIP) two to three times higher than that required to remove the bulk deposit.

The average deposit adhesion strength primarily depends on the surface temperature [6]. Figure 31 identifies the temperature zones within a typical recovery boiler, showing how the average adhesion strength of the precipitator dusts would vary within each zone. Also, study [6] shows that the contact area between a deposit and a surface is very important for the removability of the deposit attached to the tube: the smaller this interface is, the easier it is to remove the deposit.

Experimental study of ash deposition and shedding in a straw fired boiler [33] showed that in a tube-deposit system two types of adhesive contacts can be distinguished:

1. Tube - deposit interface, between the tube and the inner deposit layer.
2. Interface between the layers inside the deposit, i.e. between the initial inner layer (formed by condensation) and the thicker outer layers (formed by inertial impaction of ash articles).

3.2. Elastic Properties

Elastic properties of a material determine how a material will behave under compression forces and tension forces. These properties are the Elastic (Young's) modulus and the Possion's ratio.

3.2.1. Elastic Modulus

The elastic (Young's) modulus, E, of a material represents the relative stiffness within the elastic range. It can be determined from a stress-strain curve by calculating the ratio of stress to strain:

$$E = \frac{stress}{strain}\left[\frac{N/m^2}{m/m}\right] \tag{24}$$

The elastic modulus can be used to predict the elongation or compression of an object, as long as the stress is less than the yield strength of the material. Britlle materials have higher values of the Young's modulus compared to ductile materials.

The elastic modulus of a porous material can be related to the elastic modulus of a non-porous material, by the relationship of Mackenzie (developed for ceramic porous materials) [5]:

$$E = E_0 \cdot (1 - a \cdot p + b \cdot p^2) \tag{25}$$

where E_o is the elastic modulus of the non-porous material, p is the porosity of the sample, and a and b are the curve fitting parameters. Physically, the parameters a and b are the pore shape factors of the porous materials.

Wain et al. [5] determined the values for the elastic modulus of coal ash slags (composition and characteristics given in Appendix A) by measuring the fracture stress and the corresponding displacement. Figure 32 shows that the elastic modulus depends strongly on the deposit porosity. The elastic modulus of each slag rapidly decreases with increased porosity, the effect being most marked in the 0 – 25 % (v/v) porosity range. Although not all the samples fit equally well to equation (25), it is possible to determine E for each coal ash slag at a given porosity.

According to the experimental study [5], both the compressive strength and the elastic modulus of a slag increase if the slag porosity is less than 25 %. This value may be considered as a critical porosity level, since above 25 % the deposit mechanical properties can be predicted with a fair degree of accuracy, regardless of its composition or microstructural details. Only if the porosity falls below this value, the microstructural features of the slag will play a significant role.

3.2.2. Poisson's Ratio

Poisson's ratio, ν, is a measure of the simultaneous change in elongation, and in cross-sectional area within the elastic range during a tensile or compressive test, i.e.:

$$v = \frac{lateral\ strain}{longitudinal\ strain} = \frac{(-\Delta d/d)}{(-\Delta l/l)} \tag{26}$$

For most materials the Poisson's ratio will fall in the range $0 \leq \nu \leq 0.5$. For a perfect isotropic material, the Poisson's ratio is 0.25, with most glasses and ceramics lying between 0.20 and 0.25 [5]. For materials like wall slags, the value 0.25 can be accepted, independently of microstructure details. Young's modulus E_0 and Poisson's ratio of various dense ceramic materials are shown in Table 6 [49]. The draw back of these data is that the material porosity is not specified. A numerical approach to calculating the Young's modulus and the Poisson's ratio can be found in study [50].

3.3. Ash Viscosity

Viscosity is the primary physical property that influences the deposit strength, as shown in Figure 33. For deposit 1, with the high liquid phase viscosity, the adhesive strength is not sufficient enough to hold the deposit in place, resulting in shedding by its own weight. Deposit 2 exhibits a rapid growth and a significant deposit strength development. The viscosity is low

enough to cause significant bonding of ash particles, but not to complete melt of the deposit. The temperature of the deposit 3 is high enough to cause melting of the deposit, and shedding through flow. The viscosity of the liquid phase in this case is very low.

The viscosity depends on the chemical composition and the temperature [34]. The viscosity of a melt decreases as the temperature increases. The melt fraction in the deposit is also very important, since it influences the flow type of the deposit, i.e. if it is Newtonian or non-Newtonian flow.

According to Vargas [34], all available mathematical models for predicting the viscosity of silicates, which are categorized as Newtonian fluids, are intended for completely molten samples. Comparison of modelling and the experimental results [34], showed that the Urban model gives the best results for coal ash, but it was concluded that a general ranking of viscosity models could not be given. The valid way to select a model is to choose a model which is based on a composition interval that covers the mixture in question. For mixtures of SiO_2, Al_2O_3 and Na_2O, the Urban model gives predictions with ± 20 % error.

If a given mixture is not completely molten it will most likely not exhibit Newtonian behaviour. If the crystal fraction and their shape are known, simple models can give an indication of the overall viscosity of mixture [34].

3.4. Melting Behavior

In some cases the deposit surface temperature reaches a critical value where a running slag is formed. This may be due to either a large fraction of molten potassium salts at the surface or due to the silicates reaching a critical viscosity at which a flow initiates [12,20,35].

The melting behavior of an ash deposit will influence its rate of build-up (the sticking propensity may increase), but also the design, and the operation of the actual boiler (e.g. due to the appearance of a running slag) [10,14]. Typically, ashes and deposits do not have one specific melting point as pure compounds do, but they melt within a temperature range. Ash deposits, as most other mixtures, have two distinct melting temperatures. The first melting temperature (FMT) [10] is defined as the temperature at which the first melt appears in the deposit. As the temperature increases, the percentage of molten phase in the deposit also increases. At the complete melting point the last solid particles are dissolved into the liquid phase, and the mixture becomes completely molten.

The temperature gradient inside the deposit is determined by the heat flux, and the heat conductivity of the deposit. The steady state thickness of a deposit, d [mm], can be estimated using the following expression [10]:

$$d = \frac{1000 \cdot k \cdot (T_f - T_M)}{\alpha \cdot (T_g - T_f)} \tag{27}$$

where k [W/mK] is the thermal conductivity of a deposit, α [W/m^2K] is the heat transfer coefficient, T_f [^0C] is the flow temperature of a deposit, T_M [^0C] is the metal temperature, and T_g [^0C] is the flue gas temperature.

3.4.1. Deposit Melting in Biomass-Fired Boilers

The main elements governing the melting behavior of the deposits in biofuel-fired boilers are chlorine and potassium. Figure 34 shows the calculated dependency [10] of the melt fraction on temperature, of biomass deposit samples containing different amounts of K and Cl.

The curves in the left-side figure are calculated with 5 % (w/w) of potassium, and on the right-side figure with 3 % (w/w) of chlorine. Using the MELTEST method, Salmenoya [10] found that the content of chlorine influences the increase of melt fraction at FMT, but not the FMT. On the other hand, potassium affects FMT, but not the amount of melt at that temperature.

The deposits in biofuel-fired boilers are usually not completely molten. Figure 34 shows that the amount of melt increases with an increase in the temperature. Molten phase present in the deposit, is usually not in a direct contact with the metal surface, but the outermost deposit layer may be molten. A molten layer on the top of the deposit may effectively block the inner layer, and retard the diffusion of gases through the deposit.

3.5. Coefficient of Thermal Expansion

The coefficient of thermal expansion,α, represents expansion of material per unit length when the temperature of the material is increased by one degree. It is usually expressed in the unit of $\mu m/(m \cdot K)$. This coefficient depends on the actual temperature, with low values at low temperatures.

The thermal and the chemical compatibility between the steel surface and the deposit, influences the deposit ability to stick and remain on the surface during thermal cycling in the boiler. If the thermal characteristics, like the thermal expansion coefficient of the heat transfer surface and the deposit material are similar, the deposit will not be removed easily during the thermal cycles. Wain et al. [34] investigated coal ash slags and observed the thermal expansion coefficients in the range 5.10 to $7.12 \cdot 10^{-6}$ C^{-1}. The expansion coefficient of slags is not dependent on the porosity, but it should be related to the Na_2O and K_2O content of the slag, since the expansion of a silicate glass is controlled by the degree of continuity of the silica matrix [34]. Both Na_2O and K_2O are very effective glass network modifiers and a small addition to SiO_2 may raise the coefficient of thermal expansion significantly. The lack of any simple correlation suggests that this particular property is a complex function of both the composition and the cristallinity. The thermal expansion coefficients for some ceramic materials are given in Table 5.

3.6. Thermal Properties of Deposits

Deposit thermal properties, i.e. the thermal conductivity and the surface emissivity, characterize the heat transfer process between the flue gas and the steam inside the heat exchanger tubes. Thus, these properties indirectly influence the process of ash deposit removal. Thermal properties are strongly influenced by the deposit physical structure, i.e. the particle size distribution, the porosity and the sintering conditions. While radiative properties will depend on the surface conditions, conductive properties will depend on properties inside the deposit.

The effective thermal conductivity of porous ash deposits, which is in detailed discussed by Zbogar et al. [52], depends on the thermal conductivity of solid phase, k_s, the thermal conductivity of gas phase, k_g, the porosity, the size distribution of pores or particles, and the deposit sintering state. The properties k_s and k_g are dependent on the temperature and the chemical composition. Since the thermal conductivity of a typical deposit solid-phase is two- to three orders of magnitude greater than the one of the deposit gas-phase, heat conduction through the deposit will primarily occur through the solid phase [16]. The overall thermal conductivity is thus strongly influenced by the material porosity. The emissivity is affected by

the deposit surface conditions (i.e. weather it is fused, or particulate), the particle size and the chemical composition (i.e. the color of the deposit) [52,53].

The thermal conductivity of deposits generally increases, when the temperature increases. Figure 35 shows experimental data on the temperature dependency of a coal ash deposit thermal conductivities, as obtained by Rezaei et al. [54] (composition of the ash is given in Appendix A). It can be noticed that below the sintering point the thermal conductivity is weakly influenced by the temperature change. Here, the thermal conductivity changes primarily due to the change of the thermal conductivity of the gas phase. Figure 35 also shows that the thermal conductivity of an ash deposit during cooling is higher and not following the same trend as during heating. This is due to the irreversible changes in the physical structure and the porosity of the samples. The emissivity is affected by the temperature increase by means of surface structural changes i.e. through a particle size increase due to sintering. As Wall et al. [53] showed, below sintering temperature the emissivity of coal ash decreases when the temperature increase, and then increases sharply at higher temperatures, as sintering and fusion of the ash occur.

The effective thermal conductivity varies significantly with the deposit type [52,54]. The thermal conductivity of a fused deposit (consisting of a continuous solid phase, with discontinuous gas voids) is considerably higher than for particulate structured deposit (consisting of a continuous gas phase, with discontinuous solid particles). The initial stages of sintering are accompanied by an increase in the deposit thermal conductivity. Subsequent sintering continues to densify the deposit, but has little effect on the deposit thermal conductivity. The thermal conductivity of a slag structure is considerably higher than of a particulate structure, especially in the porosity range 0.2-0.8 [54].

3.6.1. Calculation of Thermal Conductivity of Ash Deposits

From the modeling point-of-view, since an ash deposit is a porous structure, it can be approximated with a packed bed. Thus, the thermal conductivity of an ash deposit can be roughly determined using the models for the thermal conductivity of packed beds. Unsintered (particulate) deposits should be considered as systems with a continuous gas phase and a discontinuous solid phase. Fused deposits (slags) should be considered as systems with a discontinuous gas phase (voids), and a continuous solid phase. Sintered deposits can be treated as complex systems, where both phases are continuous. The solid phase of the ash deposits can be considered as a mixture of different oxides. Most of the models are formulated as functions of the thermal conductivities of gas and solid phase, and the porosity. Literature study performed in [52] showed that the adequate model for the thermal conductivity of solid mixtures is not available.

3.7. Influence of Chemical Composition on the Deposit Shedding

Chemical composition of a deposit influences the deposit properties connected to the deposit removal, e.g. the deposit strength. Mao et al. [55] experimentally investigated removability of synthetic deposits (addressing the deposits from the kraft recovery boiler). They concluded that key-role of chemical composition is in the liquid content of fly ash particles in the flue gas, before they hit the heat transfer/deposit surface. Chemical composition also influences the liquid content of the deposit on the heat transfer surface. At higher liquid content, the deposit becomes denser and more tenacious. One of the conditions for the

formation of a strong deposit is the formation of a liquid phase, which can bind solid ash particles.

Mao et al. [55] investigated influence of chloride, potassium and carbonate on removability of deposits from kraft recovery:

- Chloride not only has a significant effect on the rate of deposit formation, but also makes the deposit much more difficult to remove. Increasing the chloride content results in a larger amount of molten phase in ash particles, which consequently forms deposits that are denser, tenacious and more difficult to remove. Among other constituents of a deposit, chloride has the most significant effect on deposit removal.
- The influence from potassium is based on its ability to drastically lower the first melting temperature of ash particles, so they will contain liquid phase at lower temperatures. The potassium effect is decreased, if the deposit does not contain chloride.
- Carbonate has only a small effect on the deposit removal.

In the study of Baxter [56] influence of some chemical species on removability of biomass and coal deposits:

- Free silica particles are slow to fuse or sinter in the deposit, so they contribute to both a deposit granular/porous nature, and to the lack of deposit strength.
- Calcium, which originates mainly from calcite, has an effect similar to free silica with respect to granularity and deposit strength, although less pronounced.

4. Industrial Shedding Techniques

Shedding is the process of deposit removal, where pieces of deposit are separated from the heat transfer surfaces. The frequency of naturally caused shedding may be increased by different techniques incorporated in the boiler operation, like sootblowing, cleaning by ultrasound, detonation waves, shot cleaning, and rapping gears. The asymptotic growth of a deposit can be changed to a periodic process, due to the use of these active methods for the deposit removal. The heat transfer between the flue gas and the working fluid is a dynamic process affected by the increase of deposit layers and by the intensity and the frequency of cleaning of heat transfer surfaces.

4.1. Sootblowing

Ash deposits, formed on convective heat transfer surfaces, are generally removed mechanically by sootblowers. Sootblowers use high-pressure water, air or steam, which impacts a deposit, and causes its failure. Deposit removal occurs due to mechanical and thermal stresses, induced in the deposit. Characteristic parameter for sootblowing is the Peak Impact Pressure, PIP, as was previously explained. The major drawback of this cleaning method is that it causes abrasion and erosion of the boiler tubes, and consumes large amounts of high-pressure steam [39,40].

Cleaning of heat transfer surfaces, which is implemented in a boiler operation, is practical as long as the ash deposits are not highly sintered or strongly attached to the surface [5,39]. Some deposits are removed almost immediately by sootblowing, leaving an almost clean tube surface. In other cases, deposits are difficult to remove, and may leave a thin coverage of deposits on which subsequent deposition takes place [5]. Thus, an understanding of the relationship between the nature of a deposit and its thermal and mechanical properties, relevant to the process of removal, may improve the current subjective approach to the

selection and location of sootblowers, increasing both the cost effectiveness and the availability of the unit.

Different sootblowing mediums are used for removing different deposits. Water is the most effective medium for removing heavily sintered or slagged deposits. The use of water creates a pressure wave, due to the liquid water that is quickly expanding to steam [24,39].

4.1.1. Sootblowing Principles

During sootblowing a high pressure steam from the sootblower hits the ash deposit, as is schematically presented in Figure 36. Sootblowing induces significant mechanical stresses in the deposit, which can lead to its failure. Sootblowing can also cause thermal shock, if there is a significantly large temperature difference between the sootblowing medium and the deposit, which would cause deposit shrinking. When a sootblower jet hits a deposit, the two major forces are induced in it [6,24], as shown in Figure 37:

- a longitudinal (drag) force, in the axial direction of the jet, and,
- a lateral (lift) force, perpendicular to the jet axis (caused by asymmetry of the deposit shape, non-uniformity of the velocity of the jet, and turbulent pulsation in the jet).

Ebrahimi-Sabet [24] discussed in details the forces acting on a deposit during sootblowing. Due to their turbulent nature, each of these forces consists of a mean component and a fluctuation component. The deposit removal is not only influenced by the magnitude of the aerodynamic forces, but also by their direction. A jet pushing the deposit onto the tube surface primarily produces compressive stresses, which rarely alone cause the deposit removal. If the force is applied from aside, substantial tensile stresses may be generated in order to cause the deposit removal. If the jet hits a deposit from the front, the lift force is much more effective in removing the deposit than the drag force, which pushes the deposit onto the surface of the tube.

4.1.2. Properties Influencing Sootblowing

The ability of a sootblower to remove deposits depends on two main factors: the Peak Impact Pressure (PIP) of the sootblower stream jet, and the deposit strength [39]. In order to remove the deposit, the PIP must be greater than the deposit mechanical strength, or the adhesion strength at the deposit-tube interface.

Shedding is directly affected by the strength development in the deposit. A non-sintered, porous deposit does not posses much strength, and it is easily swept off the surface. Sintering causes the deposit to consolidate and to build-up strength [14], which makes it more difficult to remove mechanically. Sintering is strongly influenced by the deposit particle size, the porosity and the viscosity, all of the properties being dependent on temperature. Deposit removal by sootblowing occurs rapidly for a deposit consisting of fine particles at high temperatures, and proceeds slowly for a deposit consisting of large particles at low temperatures. Considering viscosity, dry particles will not sinter together, whereas sticky particles will [34].

4.1.2.1. Effect of Tube Surface Temperature on Deposit Removability

The tube surface temperature has a significant effect on the process of deposit removal. Increasing the tube surface temperature makes deposits more difficult to remove. The PIP required for a deposit removal reaches its maximum value at a certain temperature, but when

this temperature is passed, the needed PIP value typically starts to decrease sharply, as it is shown in Figure 38. This can be explained by: 1) a high amount of melt phase decrease the deposit strength, and 2) some ash species may evaporate, and cause evaporate and cause development of large pores.

4.1.3. Stress Removability Criterion

Kaliazine et al. [6] identified the adhesion bond between the deposit and the tube surface as the breaking point during sootblowing, for deposits in the superheater region of kraft recovery boilers. A deposit is expected to be removed when the stresses at the tube-deposit interface exceeds the deposit strength. The debonding will occur when the condition expressed in equ. (16). The criterion for the brittle break-up in terms of PIP is given in equ. (15). Whereas the brittle break-up is independent of the deposit geometry, removal by debonding requires a smaller PIP as the deposit thickness increases. Experimental results on deposits in kraft recovery boilers [6] show that the deposit tensile strength is much higher than the adhesion strength between the deposit and the tube surface, i.e. $\sigma_t >> \sigma_{adh}$. Hence, the removal by debonding is more probable than the brittle break-up (in kraft recovery boilers).

Equation (15) was derived using the assumption that the pressure distribution over the deposit surface is similar to that produced by a uniform flow. It may therefore not be applicable if the jet diameter is small comparing to the deposit size, because than the jet would only hit a small spot on the deposit surface. As stated by Kaliazine et al. [39], if deposit removal includes other mechanisms than brittle break-up, then equ. (15) may overestimate the minimum PIP required to remove the deposit. For instance, if a strong deposit is weakly attached to the tube surface, it might be removed even if the PIP is less than required according to equ. (15). If the PIP satisfies equ. (15), the deposit would be removed despite any additional mechanism involved. Equ. (15) therefore provides a conservative estimate of the cleaning distance, i.e. an upper limit for the PIP required to remove a brittle deposit.

4.1.4. Analysis of Forces during Sootblowing

The sootblower jet produces both steady (mean) and fluctuating forces on the deposit [24,39]. The mean aerodynamic forces can be decomposed into a drag component, F_D (acting in the direction of flow), and a lift component, F_L (acting perpendicular to flow direction, see Figure 37. These forces are usually expressed as lift coefficients for cylindrical bodies (as is the case of a tube with a deposit):

$$C_D = \frac{F_D / LH}{\rho U^2 / 2} \qquad C_L = \frac{F_L / LH}{\rho U^2 / 2} \tag{28}$$

where C_D and C_L [-] are the drag and the lift coefficients, U [m/s] is the velocity of the flow, L [m] is the body length, H [m] is the characteristic body width (for a clean tube, without a deposit, and H is the tube diameter).

The fluctuating component of the drag force is usually small in comparison to its mean value, therefore the drag force may be considered as a steady force. The lift force has a mean value usually much lower than the drag force, and for a symmetrical body, the mean lift force is zero. But, the fluctuating lift force is usually quite big, and it is comparable in magnitude to the mean drag force. The fluctuating force is expressed by its mean-squared value:

$$F' = \sqrt{\frac{1}{T}\int_0^T F^2(t)dt} \tag{29}$$

For fluctuating forces, the aerodynamic coefficients are also used:

$$C'_D = \frac{F'_D / LH}{\rho U^2 / 2} \qquad C'_L = \frac{F'_L / LH}{\rho U^2 / 2} \tag{30}$$

Experimental data for C_D and C_L [24] are available mainly for bodies immersed in a subsonic, uniform, parallel flow. For a single tube, C_D is 0.5 – 2, while C_L' varies from 0.12 to 4 (typically, high values of the lift coefficient have been observed in narrow passages and tube banks).

The total drag force coefficient of a long single circular tube reaches a constant value $C_D \approx 1.2$, for a Re number from 1000 to $2 \cdot 10^5$ [24]. At $Re_{cr} \approx 2 \cdot 10^5$ the locus of the boundary layer separation is shifted downstream for a cylinder with a smooth surface, as the boundary layer changes from laminar to turbulent. The occurrence of turbulence in the boundary layer on a cylinder causes a decrease in the drag coefficient, C_D to approximately 0.32. With a further increase in the Reynolds number to supercritical values, the locus of the transition to a turbulent boundary layer shifts upstream. Therefore, the value of C_D at the supercritical Re is slightly higher than at the critical Re, and it increases to an average value of 0.42. However, this stands only for cylinders with very smooth surfaces and for turbulence-free flow. If a cylinder has a rough surface, the roughness disturbs the flow near the surface, the transition to turbulence occurs at smaller Re, and the corresponding decrease in the drag coefficient shifts accordingly. The larger is the equivalent roughness, k_s, the greater is the shift. If the relative roughness, $k_s \cdot d$, is greater than 0.01, the drag force coefficient varies within the limits 0.9 – 1.2 for all Re>1000. For operating conditions where Re numbers are very large (as in boilers) the mean drag coefficient is independent of Re number variations [40].

The amplitude of the mean lift coefficient C_L depends strongly on the deposit geometry and orientation. It equals zero for symmetrical deposits with respect to the jet axis [24]. When the tubes are arranged in a bundle, the drag and the lift coefficients changes, and they depend on the position of the tube in the bundle and on the bundle geometry.

4.2. Other Industrial Cleaning Techniques

Surface areas in a utility boiler can be cleaned using sound waves, i.e. acoustic cleaning. Sonic waves induce fluctuations in a flowing gas, forcing the particles within the gas to oscillate. This motion loosens an ash deposit. Sound waves are highly reflective, eliminating the possibility of particulate accumulation in blind spots, which is sometimes the case with the mechanical methods, such as sootblowing and rapping gears. The gentle nature of acoustic cleaning methods does not cause harm to heat transfer surfaces, as does high pressure-, high velocity fluid (steam or air). The use of acoustics significantly decreases down-time, reduces the boiler wear, and minimizes steam- and compressed air consumption. The most common type of horn works at frequencies between 125 to 250 Hz [57]. The number of horns needed in any installation is based on the size and the configuration of the boiler, and the ash build-up rate.

Detonation wave techniques can be efficiently applied for removing various types of industrial equipment exposed to heavy fouling [58]. The basic principal of the detonation wave

cleaning technique relies on the utilization of shock waves, generated by the detonation of the fuel-oxidant mixture in a special chamber, i.e. detonation chamber, placed outside the equipment to be cleaned. After reaching the position beyond which there is no energy supply, i.e. at the end of the fuel-oxidant mixture zone, or at the most at the entry of the boiler interior, the detonation wave transforms into a shock wave, which propagates into the non-reactive environment and impacts on the exposed surface. This impact action and associated effects produce the desired breakage and removal of the deposit from the impacted surface. Side effect of deposit removal by a detonation wave is the potential damage caused by vibration.

Heat transfer surfaces in a boiler can also be cleaned using the small particles (available in different geometries), by so called shot cleaning [59]. The shot is held in a hopper above the boiler, and is dropped down onto a distributor, that re-directs the particles throughout the top of the boiler. Shot cleaning may result in tube erosion, if the shot hits bare tubes.

Rapping gears [59] are mainly employed for horizontal boiler sections, in waste incineration plants. Rapping is done mechanically on the strengthened back of horizontally arranged headers. The beating energy sets the upright suspended heating surfaces into vibration and thus cleans the dirt off them.

5. Conclusion

Formation of ash deposit is a significant problem which occurs during combustion of different solid fuels. Ash deposits decrease the boiler thermal efficiency, since they act as a heat resistance for heat transfer between flue gases and a working fluid. They may also cause serious operational problems, like decreasing or completely blocking the paths of the flue gas through the boiler. Thus, it is of great interest for boiler operators to know more about deposit formation and removal mechanisms, which could be used for optimizing the boiler operation in terms of better controlled deposition process.

The aim of this literature study was to make an overview of the present knowledge about the shedding of fireside ash deposits, and the properties which affect it. Shedding is a process of ash deposit removal from the heat transfer surfaces, which can be caused naturally or artificially. The following mechanisms were identified as naturally caused shedding: erosion, gravity force (including melting), and thermal stresses. Artificially caused shedding is based on deliberately induced erosion, thermal and mechanical stresses, which is done by implementing different techniques into the boiler operation. Usually, artificial shedding occurs in parallel to natural shedding, in order to make the deposit removal more efficient. Relevant physical properties, which influence the process of deposit shedding, are: tensile and adhesion strength, elastic properties, viscosity, thermal expansion coefficient, melting behavior, thermal properties.

The special interest of this study was the process of ash deposition and shedding in biomass boilers. The general conclusion is that the fundamental knowledge about deposit shedding in biomass boilers is limited. Some data exists for shedding of coal deposits, while the shedding of deposits in kraft recovery boilers was systematically studied. Due to specific composition (they consist solely of alkali salts), the data from the kraft recovery boilers cannot be strait-forwardly used, but they can be used as a starting point for future studies.

The knowledge about the deposit properties, relevant in the deposition and shedding processes, and their modeling is limited. In many cases data and models for the ceramic materials has to be applied.

References

[1] Sander B. Properties of Danish fuels and the requirements for power production. Biomass and Bioenergy 1997; 12 (3): 177-183.
[2] Obernberger I. Decentralized biomass combustion: State-of-the-art and future development. Biomass and Bioenergy 1998; 14: 33-56.
[3] Jensen P, Stenholm M, Hald P. Deposit investigation in straw-fired boilers. Energy & Fuels 1997; 11: 1048-1055.
[4] Jensen P, Frandsen FJ, Hansen J, Dam-Johansen K, Hensriksen N, Hoerlyck S. Stenholm M, Hald P. SEM investigation of superheater deposits from biomass-fired boilers. Energy & Fuels 2004; 18: 378-384.
[5] Wain SE, Livinston WR, Sanyal A, Williamson J. Thermal and Mechanical Properties of Boiler Slags of Relevance to Sootlowing. Proceedings: Inorganic Transformations and Ash Deposition During Combustion, ed.SA Benson. Florida, 1991.
[6] Kaliazine A, Tran H, Cormack DE. The Mechanisms of Deposit Removal in Kraft Recovery Boilers. Journal of Pulp and Paper Science 1999; 25
[7] Piroozmand F, Tran H, Kaliazine A, Cormack D. Strength of recovery boiler fireside deposits at high temperatures. Tappi Proceedings 1998; 1:169-179.
[8] Tran HN, Barham D, Reeve DW. Sintering of fireside deposits and its impact on plugging in kraft recovery boilers. Tappi journal 1988; April: 109-113.
[9] Laursen K, Frandsen F, Larsen OH. Ash Deposition Trials at Three Power Stations in Denmark. Energy & Fuels 1998; 12, 429-442
[10] Salmenoya K. Field and laboratory studies on chlorine-induced superheater corrosion in boiler fired with biofuels. Abo Akademi, Finland, 2000.
[11] Frandsen FJ. Utilizing biomass and waste for power production—a decade of contributing to the understanding, interpretation and analysis of deposits and corrosion products. Fuel 2005; 84, 1277–1294
[12] Walsh PM, Sayre AN, Loehden DO, Monroe LS, Beer JM, Sarofim AF. Deposition of Bituminous coal Ash on an Isolated Heat Exchanger Tube: Effects of Coal Properties on Deposit growth. Prog. Energy Combust. Sci 1990; 16: 327- 34
[13] Andersen KH. Deposit formation during coal-straw co-combustion in a utility pf-boiler. PhD Thesis. DTU, 1998.
[14] Hansen L. Melting and sintering of ashes. PhD Thesis. DTU, 1998.
[15] Nowok JW. Densification, shrinkage and strength development in selected coal ashes. Journal of the Institute of Energy 1996; 69: 9-11.
[16] Robinson AL, Buckley SG, Baxter LL. Experimental measurements of the thermal conductivity of ash deposits: Part 2. Effects of sintering and deposit microstructure. Energy&Fuels 2001; 15 (1): 75-84.
[17] Bernath P, Sinquefield SA, Baxter LL, Sclippa G, Rohlfing CM, Barfield M. In situ analysis of ash deposits from blac liquor combustion. Vibrational Spectroscopy 1998; 16: 95-103
[18] Miles TR, Miles TR Jr, Baxter LL, Bryers RW, Jenkins BM, Oden LL. Boiler deposits from firing biomass fuels. Biomass and bioenergy 1996; 10 (2-3): 125-138
[19] Couch G. Understanding aslagging and fouling in pf combustion. IEA Coal Research, Report No. IEACR/72, August 1994

[20] Nielsen HP. Depostion and high temperature corrosion in biomass-fired boilers. PhD Thesis. DTU, 1998.
[21] Benson SA, Jones ML, Harb JN. Ash formation and deposition, In: Fundamentals of Coal Combustion for Clean and Rfficient Use, edited by LD Smooth, Elsevier, Amsterdam, 1993
[22] Hansen LA, Nielsen HP, Frandsen FJ, Dam-Johansen K, Hoerlyck S, Karlsson A. Influence of deposit formation on corrosion at a straw-fired boiler. Fuel Processing Technology 2000; 64 (1-3): 189-209.
[23] Stitt S, Junker H, Baxter LL. Optimisation of Deposit Removal in Biofueled Boilers: Review of Control Systems, Technologies and Mechanisms. Project No. Eltra 3144; TW 13317.00. 2002.
[24] Ebrahimi-Sabet SA. A Laboratory study of deposit removal by debonding and its application to fireside deposits in kraft recovery boiler. Ph.D.Thesis. University of Toronto, 2001.
[25] Raask E. Mineral impurities in coal combustion. Hemisphere publishing corporation, Washington, 1985.
[26] Raask E. (1988). 'Erosion wear in coal utilization', Hemisphere publishing corporation
[27] Latella BA, O'Connor BH. Effect of porosity on the erosive wear of liquid-phase-sintered alumina ceramics. J.Am.Soc 1999; 82(8): 2145-2149.
[28] Oka YI, Yoshida T. Practical estimation of erosion damage caused by solid particle impact. Part 2: Mechanical properties of materials directly associated with erosion damage. Wear 2005; 259: 102–109
[29] Oka YI, Ohnogy H,Hosokawa T, Matsumura M. The impact angle dependence of erosion damage caused by solid particle impact. Wear 1997; 203-204: 573-579.
[30] Sundararajan G, Roy M. Solid particle erosion behavior of metallic materials at room and elevated temperatures. Tribology International 1997; 30(5): 339-359.
[31] Oka YI, Okamura K, Yoshida T. Practical estimation of erosion damage caused by solid particle impact. Part 1: Effects of impact parameters on a predictive equation. Wear 2005; 259: 95–101
[32] Oka YI, Matsumura M, Kawabata T. Relationship between surface hardness and erosion damage caused by solid particle impact. Wear 1993; 162-164: 688-695
[33] Zbogar A. Jensen PA, Frandsen FJ, Hansen J, Glarborg P. Experimental Investigation of Ash Deposit Shedding in a Straw-Fired Boiler. Energy & Fuels 2006; 20(2): 512-519
[34] Vargas S. Straw and coal ash rheology. PhD Thesis. DTU, 2001.
[35] Kaer SK. Numerical investigation of deposit formation in straw-fired boilers. PhD Thesis. Alborg University, Denmark, 2001
[36] Hecken M, Reichelt L, Renz U. Numerical simulation of slagging films in the pressurized coal combustion facility Aachen. In: Proceeding of the 4th International Symposium on Coal Combustion, Peking, 1999.
[37] Holland L. The properties of glass surfaces. London, Chapman and Hall, 1964
[38] Hull AW, Burger EE, Navias L. Glass to metal seals. Jour. Appl. Phys.1941; 12:698
[39] Kaliazine A, Cormack DE, Piroozmand, Tran H. Sootblower optimisation II: Deposit and sootblower interaction. Tappi journal 1997; 80(11).
[40] Jameel MI, Cormack DE, Tran H, Moskal TE. Sootblower optimization – Part 1: Fundamental Hydrodynamics of Sootblower Nozzle and Jet. Tappi J. 1994; 77(5): 135-142
[41] Kaliazine A, Cormack DE, Ebrahimi-Sabet A, Tran H. The mechanics of deposit removal in kraft recovery boilers. In: Proc. Intl. Chem. Rec. Conf., Tampla, FL, 2: 641-654, 1998
[42] Ceramics for Non-Ceramists. Material Engineering Courses MMAT 382 Ceramics I and MMAT 482 Ceramics II. University of British Columbia.

http://www.mmat.ubc.ca/courses/mmat382/
[43] Hasselman DPH. Micromechanical thermal stresses and thermal stress resistance of porous brittle ceramics. J.Amer.Ceram.Soc 1969; 52(4): 215-216.
[44] Hasselman DPH. Griffith criterion and thermal shock resistance of single-phase versus multiphase brittle ceramic. J.Amer.Ceram.Soc 1969; 52 (5): 288-289.
[45] Hasselman DPH. Griffith flaws and the effect of porosity on tensile strength of brittle ceramics. J.Amer.Ceram.Soc. 1969; 52(8): 457.
[46] Hasselman DPH. Crack growth and creep in brittle ceramics. J.Amer.Ceram.Soc 1969; 52 (9): 517-518.
[47] Hasselman DPH. Unified theory of thermal shock fracture initiation and crack propagation in brittle ceramics. J.Amer.Ceram.Soc 1969; 52 (11): 600-604.
[48] Ryshkewitch E. Compression Strength of Porous Sintered Alumina and Zirconia. Journal of American Ceramic Society 1953; 36: 65.
[49] Kamiya H, Sekiya Y, Horio M. Thermal stress fracture of rigid ceramic filter due to char combustion in collected dust layer on filter surface. Powder Technology 2001; 115:139-145
[50] Roberts AP, Garboczi EJ. Elastic properties of model porous ceramics. Journal of American Ceramic Society 2000; 83 (12): 3041-3048
[51] Benson SA. Ash Formation and Behavior in Utility Boilers.
http://www.microbeam.com/Articles/Articles.htm
[52] Zbogar A, FrandsenFJ, Jensen PA, Glarborg P. Heat transfer in ash deposits: A modelling tool-box. Progress in Energy and Combustion Science 2005; 31: 371–421
[53] Wall TF, Bhattacharya SP, Zhang DK, Gupta RP, He X. The properties and thermal effects of ash deposits in coal-fired furnaces. Prog Energy Combust Sci 1993;19:487–504.
[54] Rezaei HR, Gupta RP, Bryant GW, Hart JT, Liu GS, Bailey CW, Wall TF, Miyamae S, Makino K, Endo Y. Thermal conductivity of coal ash and slags and models used. Fuel 2000; 79: 1697-1710
[55] Mao X, Tran H, Cormack DE. Effects of Chemical Composition on the Removability of Recovery Boiler Fireside Deposits. Tappi journal; 84(6)
[56] Baxter LL. Ash deposition during biomass and coal combustion: A mechanistic approach. Biomass and Bioenergy 1993; 4 (2): 85-102
[57] Buhl L, Drue S, Lind L. Field testing of acoustical cleaning of electrostatic precipitators. FLS miljo a/s, Denmark
[58] Hanjalic K, Smajevic I. Detonation-wave technique for on load deposit removal from surfaces exposed to fouling: Part 1-Experimental investigation of the method. Journal of engineering for gas turbines and power 1994; 116: 223-320
[59] http://www.rosink.com
[60] Hodgman CD. (ed.) Handbook of chemistry and Physics. Cleavland, Ohio, 1962

Component	Bituminous coal ash	Cereal straw ash
	Wt %	Wt %
Ash content in fuel	5-20	2-7
SiO_2	40-60	38
Al_2O_3	20-35	0,2
Fe_2O_3	2-15	0,3
CaO	0-10	12
MgO	0-4	3
K_2O	0-4	30
Na_2O	0-1	1
Cl	<0,5	9

Table 1. Typical ash composition for bituminous coal and cereal straw [34].

	Description	Thickness
1	a thin layer of Fe/Cr-oxide	40 – 80 μm
2	a thin dense layer of K_2SO_4 with 'threads' of Fe_xO_y in it	40 – 100 μm
3	a thickner porous layer of KCl	0.2 – 2.0 mm
4	a quite thick massive layer of KCl	0.3 – 1.5 mm
5	a quite thick massive layer of KCl with inclusions of ash particles	0.4 – 2.0 mm
6	a porous layer consisting of sintered fly ash particles	0.2 – 5.0 mm

Table 2. Layered structure of mature deposits, sintering with the innermost layer just next to the base metal [22].

Deposit removal mechanism		Where the deposit sheds		
		Tube-deposit interface	Within the deposit	Surface removal
A	Erosion			X
B	Gravimetric	X	X	
C	Melting			X
D	Thermally induced tension a) by combustion fluctuations b) by load changes c) by soot blowing	X	X	
E	Mechanically induced tensions a) (Natural) mechanical fluctuations b) Soot blowing	X	X	

Table 3. Deposit removal mechanisms

Mechanism	Deposit type			
	Powdery	Lightly sintered	Heavily sintered	Running slag
Erosion	Primary	Some	-	-
Gravimetric	Primary	Some	-	-
Melting	-	-	-	Primary
Thermal shock	-	Some	Primary	-
Mechanical shock	Primary	Primary	Some	-

Table 4. Deposit removal mechanisms (according to [23])

Material	Thermal expansion, α [10^{-6}/K]
Steels	
Mild and ferritic steels	11-12
Austenitic steels	16-18
Oxides	
Tube metal oxides (Fe_3O_4, Cr_2O_3, NiO)	8-10
Deposit constituents	
Glassy material	6-9
Quartt (crystalline)	5-8
Silicates in fired brick	7-8

Table 5. Thermal expansion coefficient of boiler-tube steels, oxides, and silicate constituents of ash deposits [6 0].

	Cordierite	Mullite	Alumina	SiC
Young's modulus (dense), E_0 [Gpa]	139	220	400	408
Bending strength (dense), σ_{FO} [Mpa]	130	220	420	409
Poisson ratio, ν	0.31	0.27	0.25	0.138

Table 6. Thermal and mechanical properties of various dense and porous ceramic material [49].

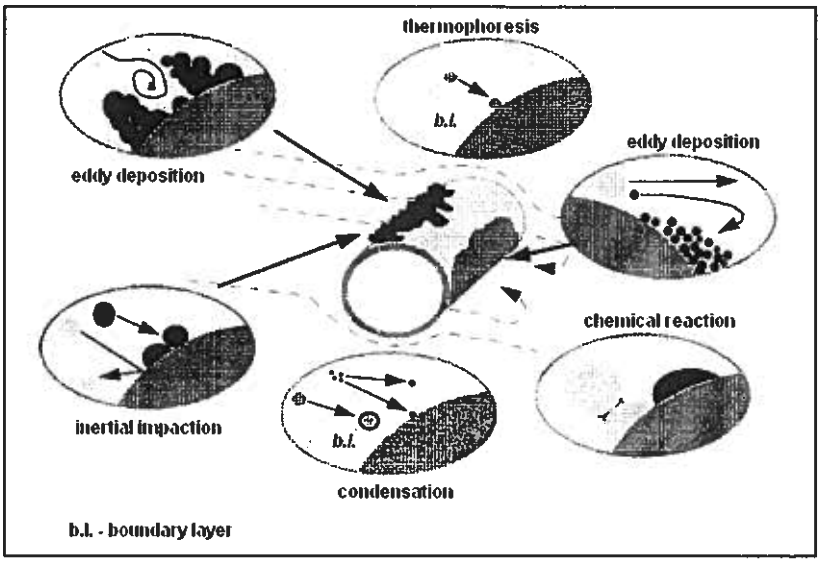

Figure 1. Mechanisms controlling deposition and maturation of ash deposits [9]

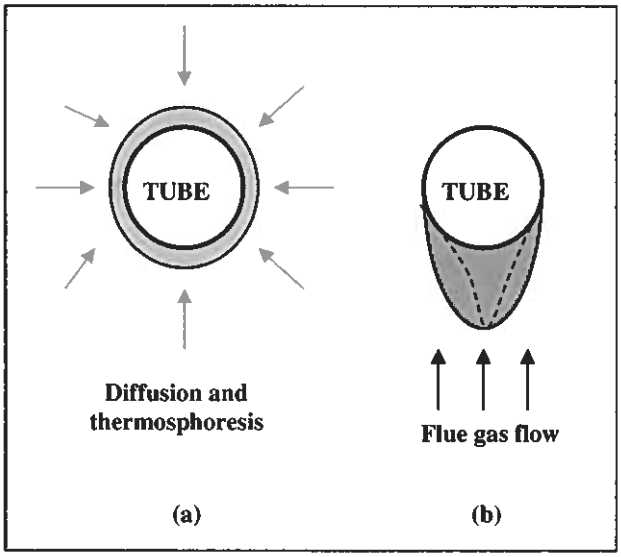

Figure 2. Formation of ash deposit on the superheater tube.

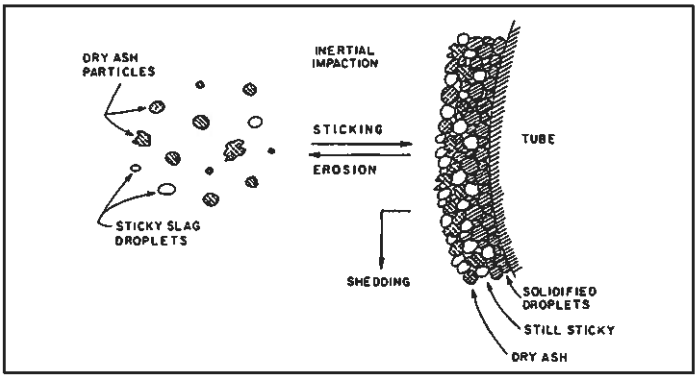

Figure 3. Processes contributing to ash deposit growth and removal [12]

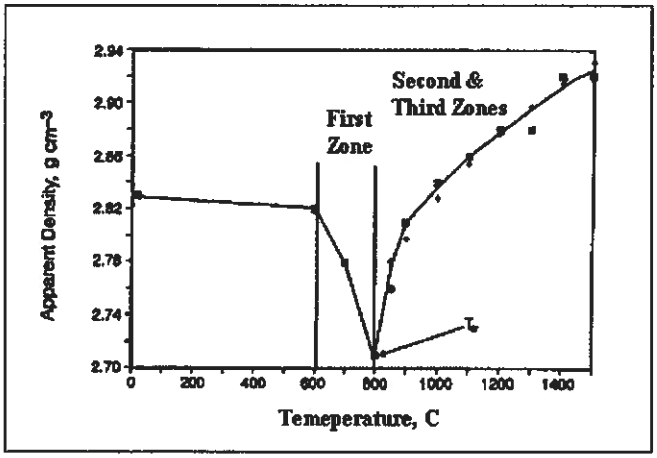

Figure 4. Variation of apparent density with sintering temperature for amorphous Beulah coal ash [15].

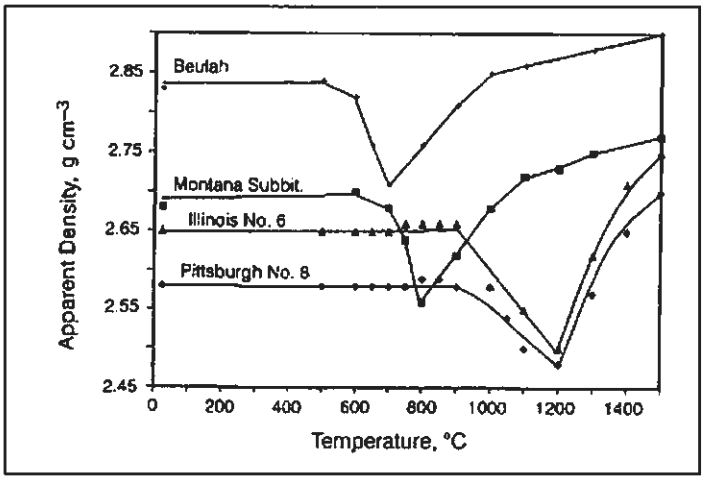

Figure 5. Relationship between apparent density and sintering temperature for various coal ashes. Ashes were sintered for 5 hours [15]

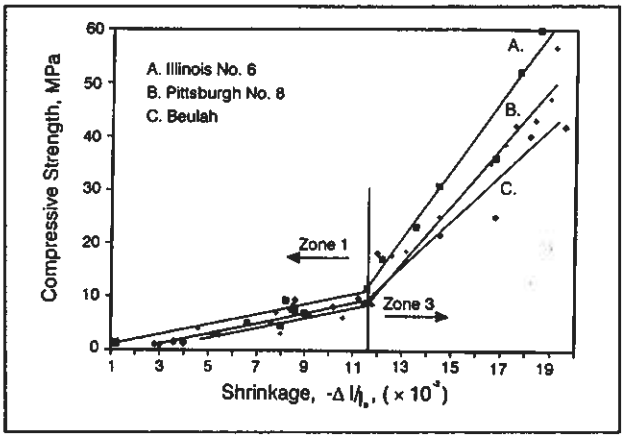

Figure 6. Compressive strength versus shrinkage for three coal ashes sintered at temperature higher than the characteristic temperature T_{cr} [15]

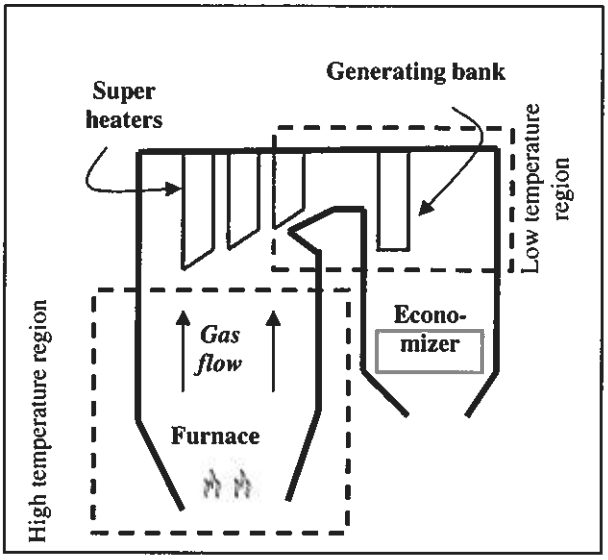

Figure 7. Scheme of a kraft recovery boiler

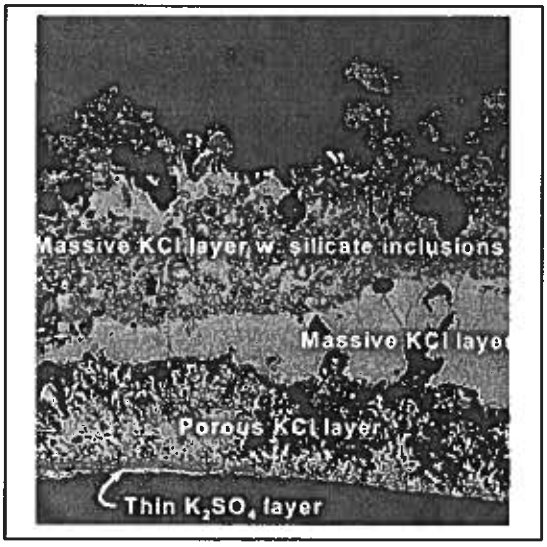

Figure 8.
SEM-micrograph showing typical deposit structure for mature deposits [22].

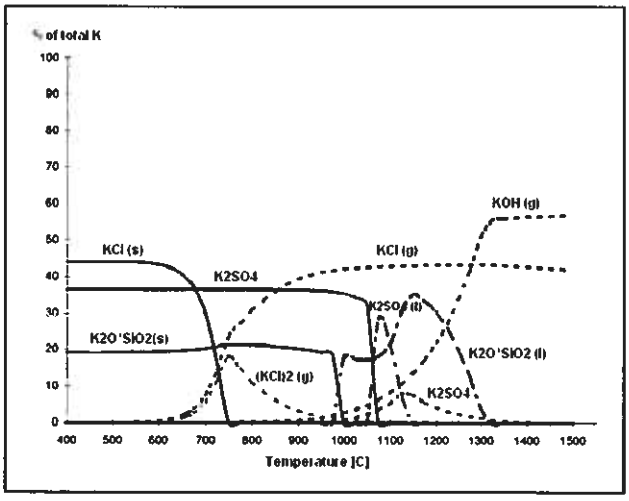

Figure 9.
Thermodynamically stable species in wheat straw combustion. S = solid phase, l = liquid phase, g = gas phase [14]

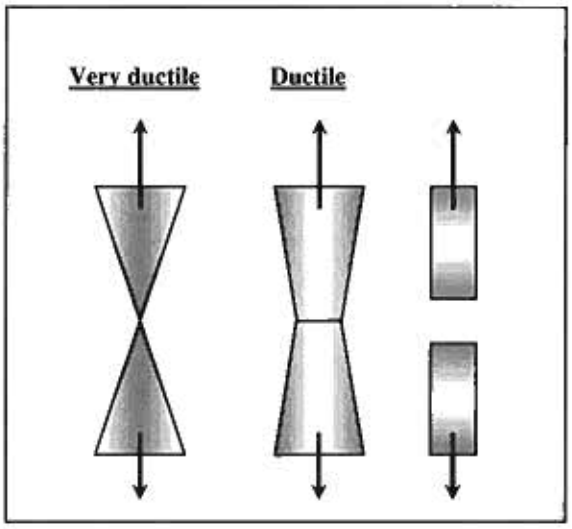

Figure 10.
Difference between brittle and ductile materials

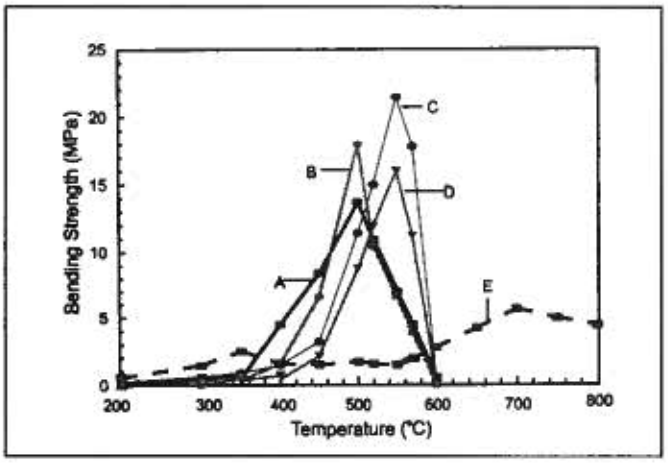

Figure 11.
Bend strength of dust pellets sintered for 4 hours at different temperatures, and tested at the sintering temperature [7]

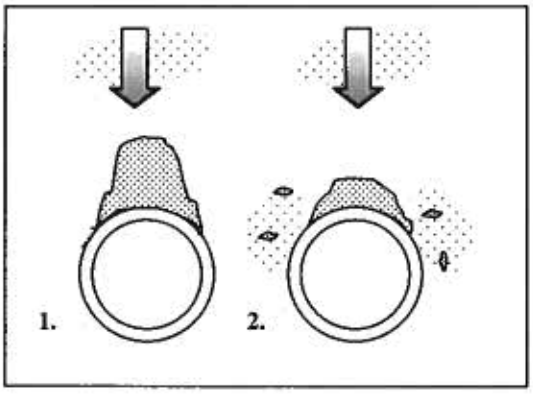

Figure 12.
Deposit erosion mechanism: 1. Deposit on tube
2. Deposit erosion process (according to [23])

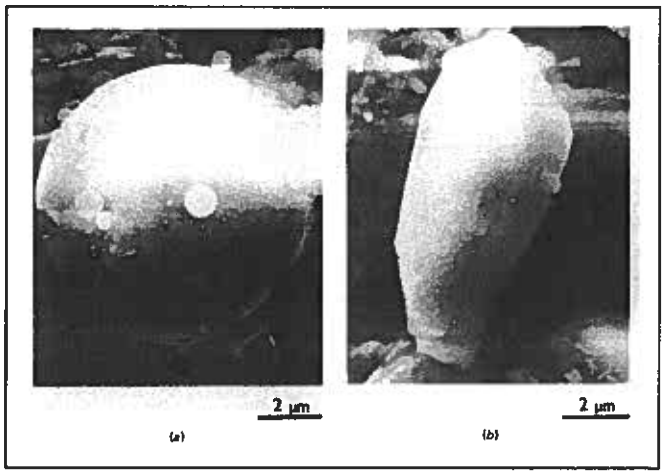

Figure 13.
The surface characteristics of spherodized and unfused particles in pulverized ash.
(a) aluminosilicate particle. (b) quartz particle
[25]

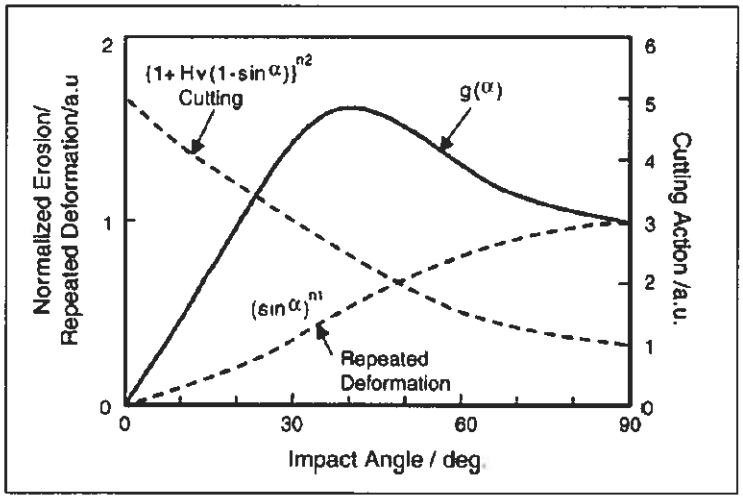

Figure 14. The concept of erosion arising from repeated plastic deformation and cutting action [31]

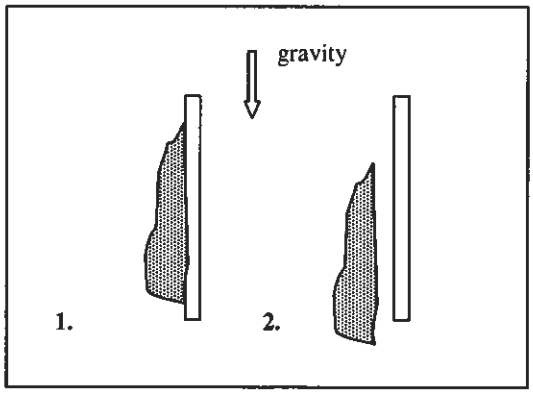

Figure 15.
Gravity shedding mechanism: 1. Deposit on the tube
2. Deposit sheds of the tube because of gravity force
(according to [23])

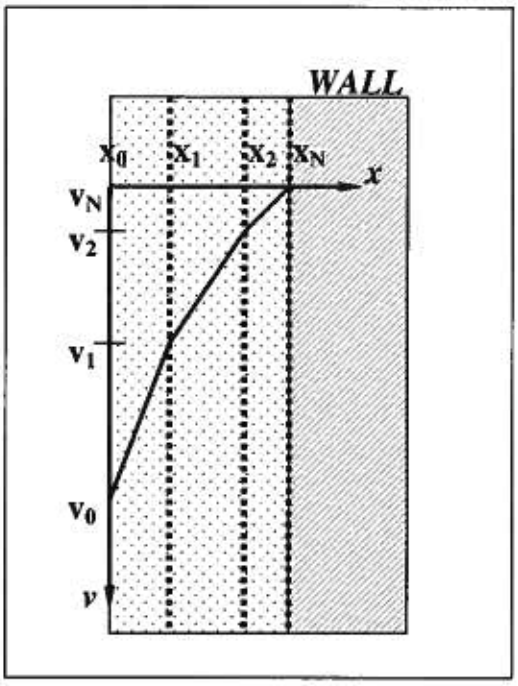

Figure 16.
Sub-layers of homogeneous composition and temperature for melting modelling [34].

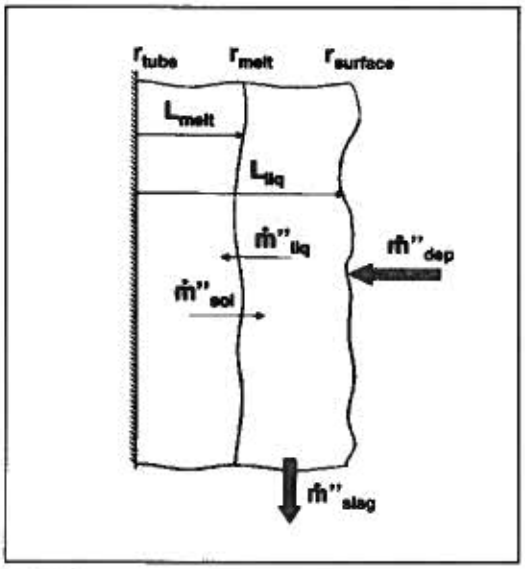

Figure 17.
Schematic illustration of a tube with the mass flux balance solved by the numerical model [35].

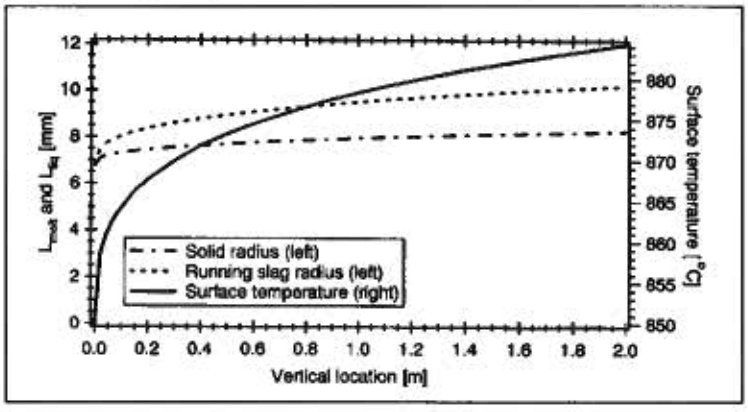

Figure 18.
Steady state thickness of solid and liquid (running slag) layers are shown on the left hand wide axis and surface temperature on the right [35]

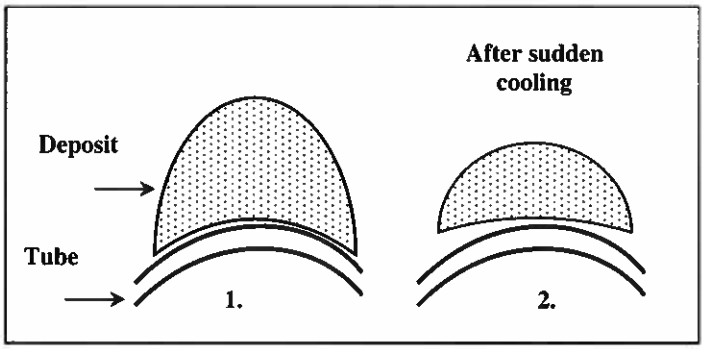

Figure 19.
Thermal shock mechanism:
1. Deposit on tube,
2. Shrinkage of the deposit

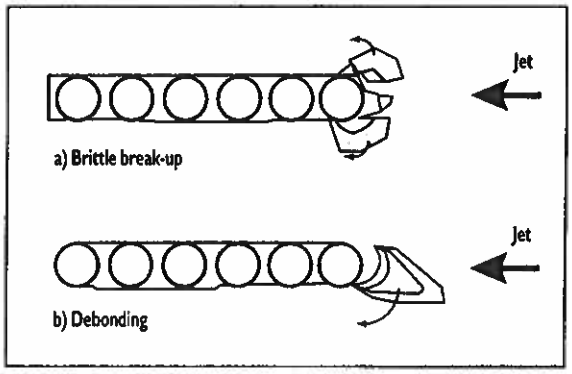

Figure 20.
Two mechanisms of deposit removal [39]

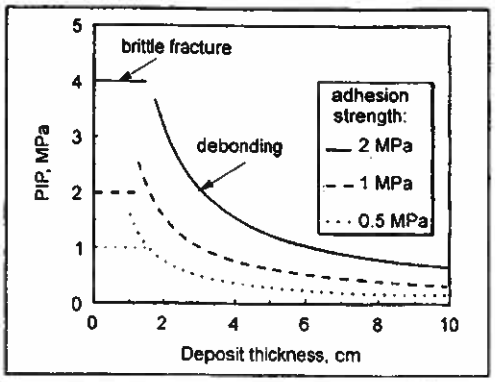

Figure 21.
PIP required to remove deposit by brittle fracture and by debonding [6].

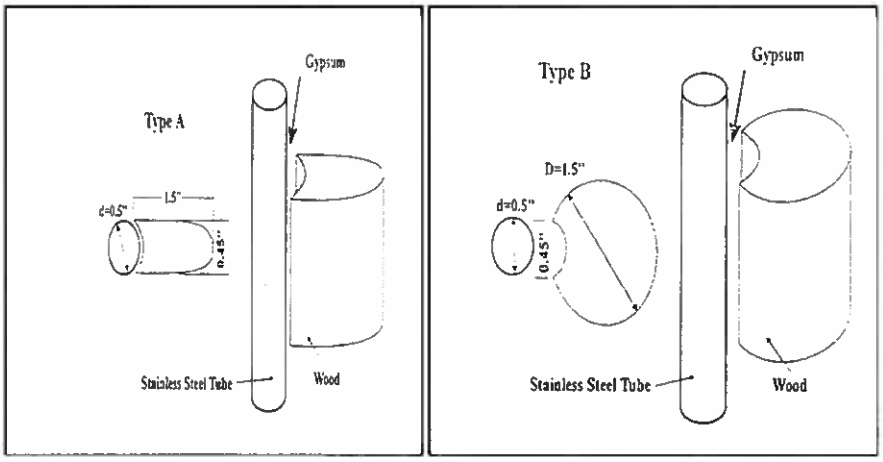

Figure 22.
Deposit models:
a) Type A
b) Type B
[24]

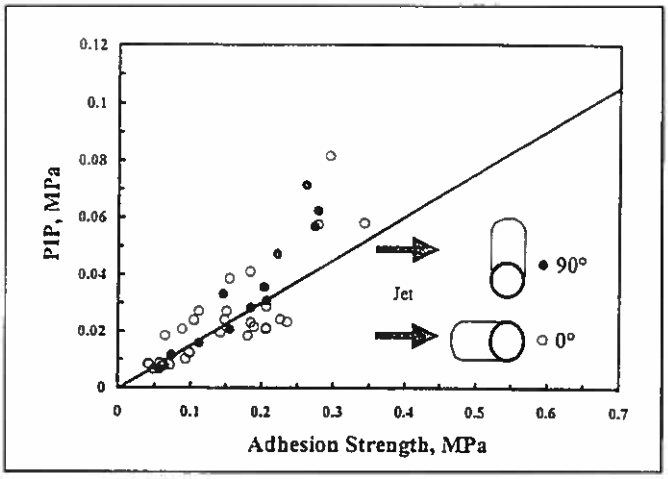

Figure 23.
PIP required to debond Type A deposit as a function of the adhesion strength [24]

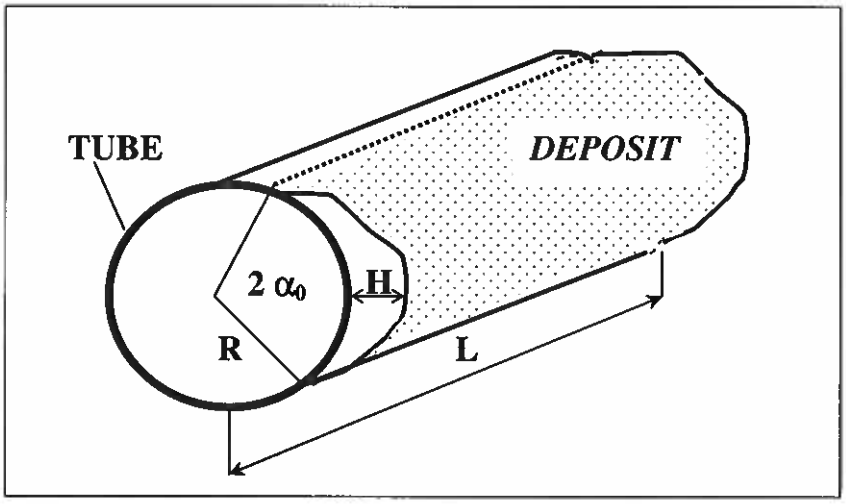

Figure 24.
Deposit and tubes geometry

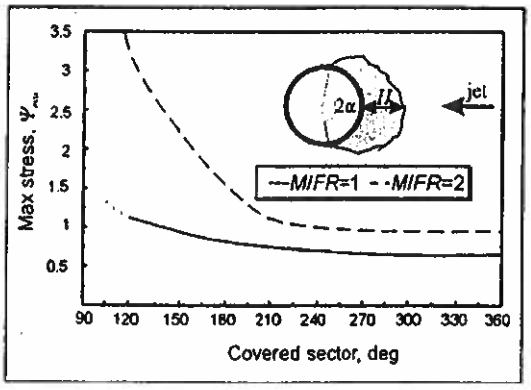

Figure 25.
Maximum dimensionless stress at deposit-tube interface as a function of covered angle [6]

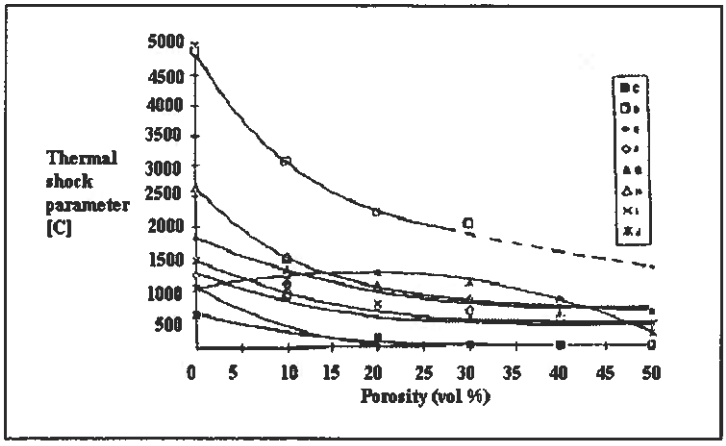

Figure 26.
Variation in thermal shock parameter R, calculated for different coal slags at porosity values from 0 to 50% [5]

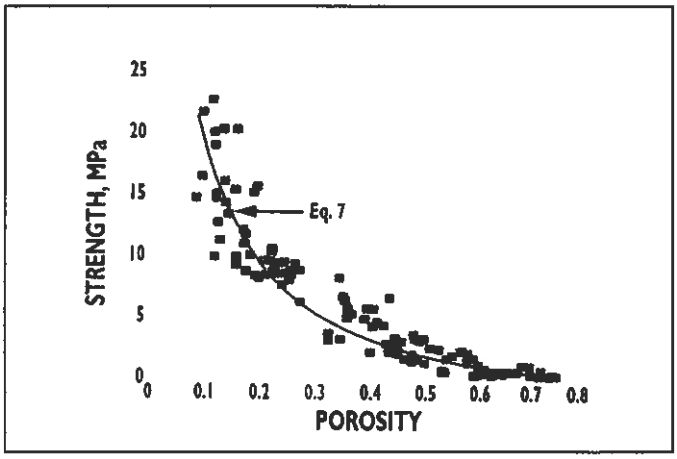

Figure 27.
Tensile strength of recover boiler deposits as a function of porosity [39]

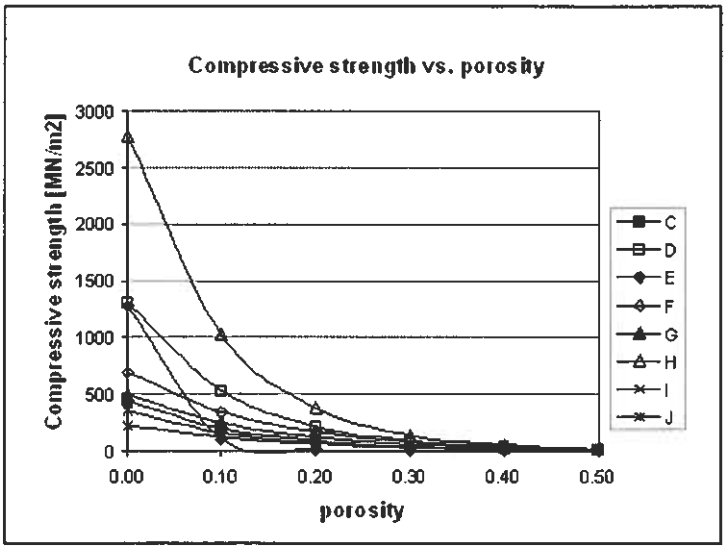

Figure 28.
Calculated values for the compressive strength of each slag as a function of porosity [5].

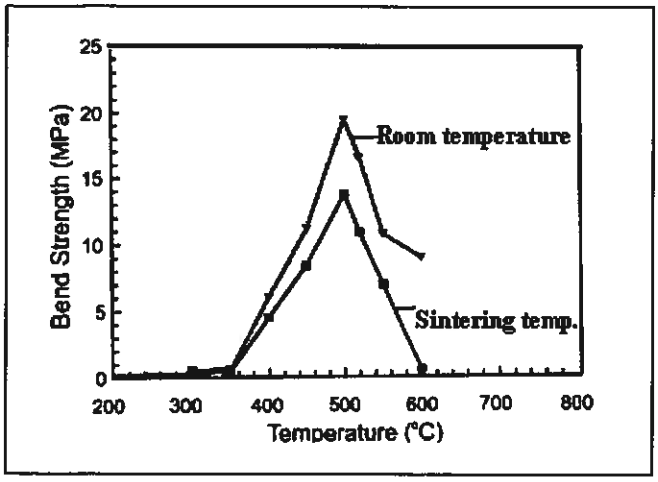

Figure 29.
Comparison between high temperature bend strength of ash dust, sintered for four hours at different temperatures and bend strength values measured at room temperature [7]

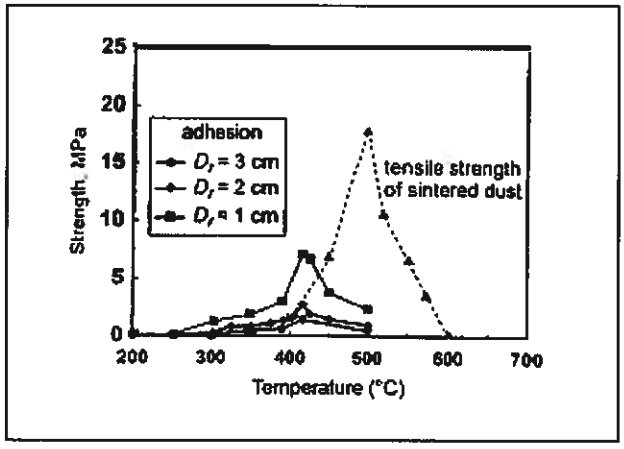

Figure 30.
Deposit adhesion strength and deposit tensile strength as a function of temperature [6]

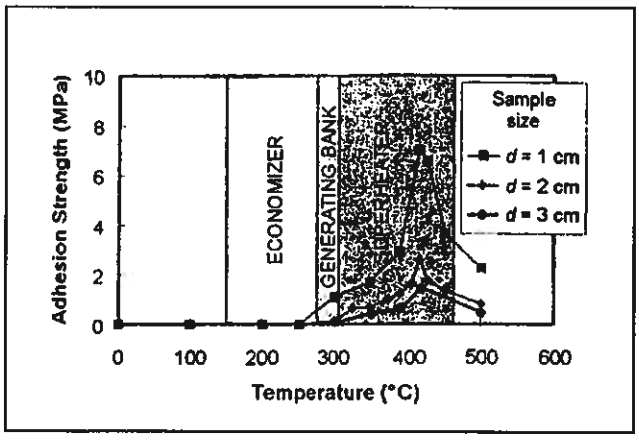

Figure 31.
Adhesion strength vs. tube temperature in the different zones typical of recovery boilers [6]

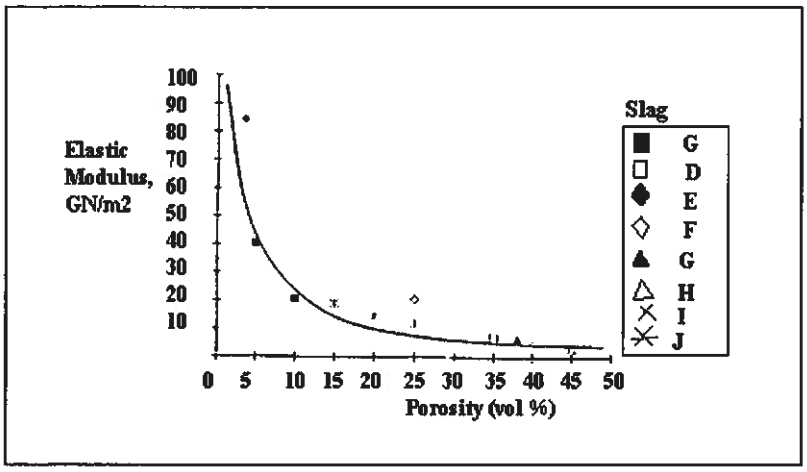

Figure 32.
Elastic modulus of different coal slags as a function of the typical porosity of that specimen [5].

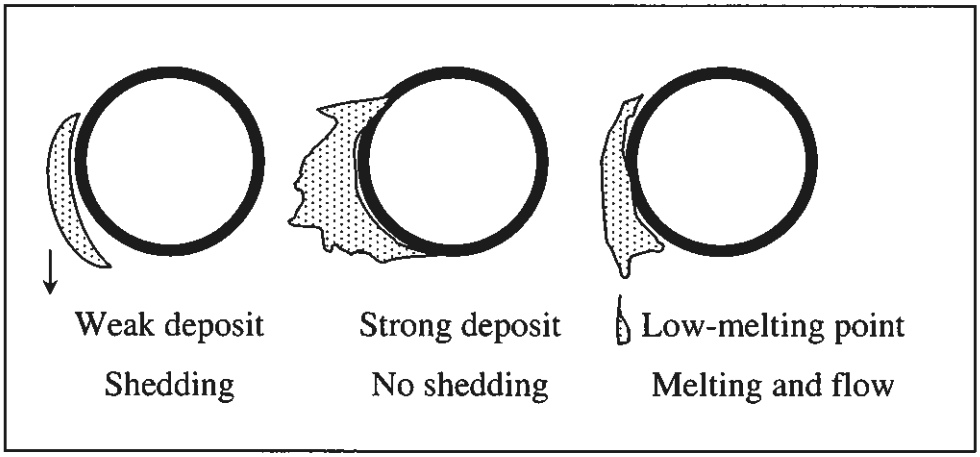

Figure 33. Relationship between deposit viscosity and strength [51]

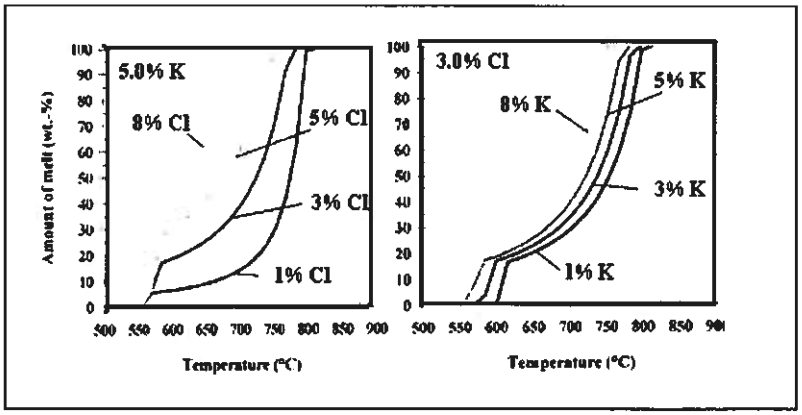

Figure 34.
Effect of chlorine(left) and potassium (right) content on ash melt fraction [10].

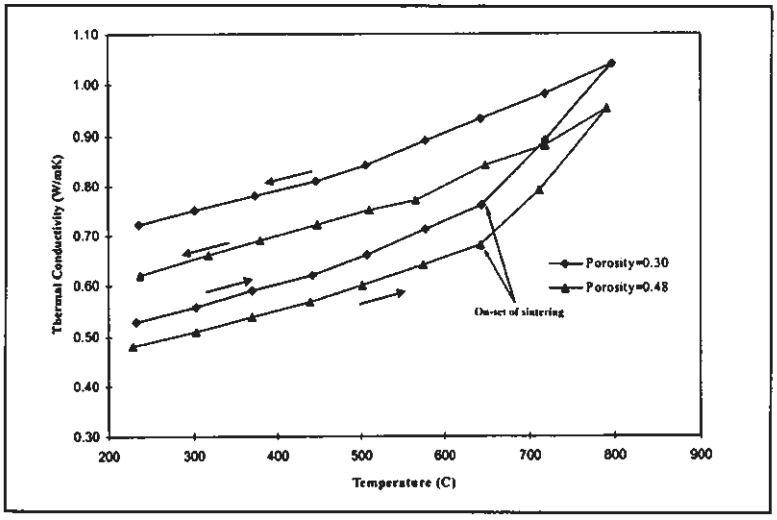

Figure 35.
Effect of temperature on thermal conductivity of coal ash (the arrows indicating heating and cooling) [54]

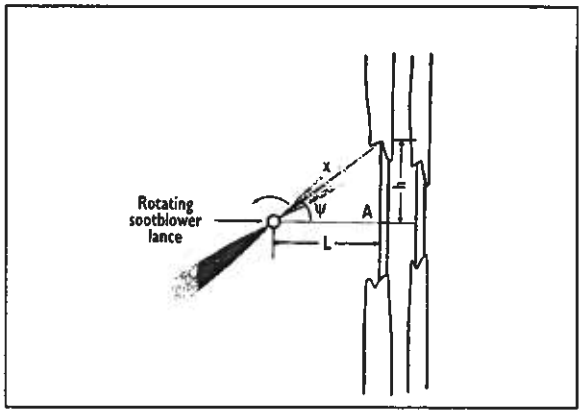

Figure 36.
Interaction of a sootblower jet with tubes [39]

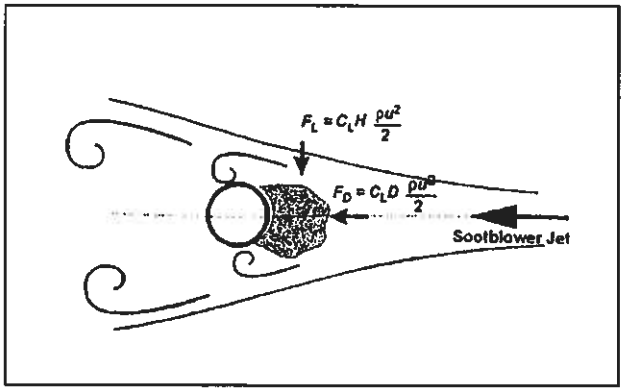

Figure 37.
Sootblower jet-deposit interaction [39]

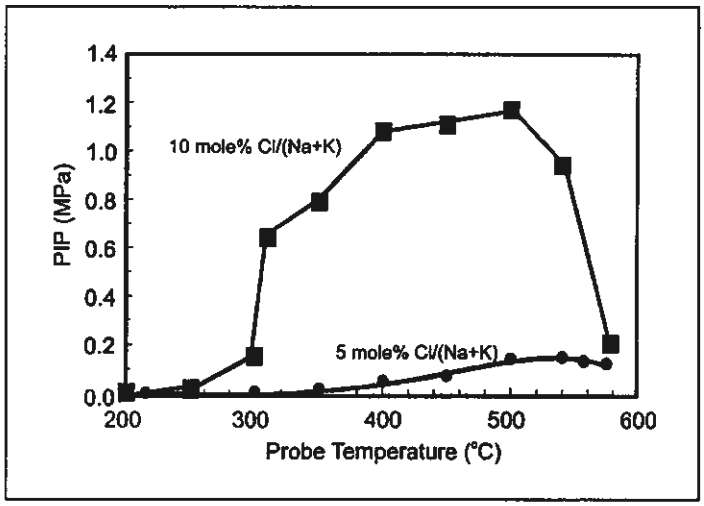

Figure 38. Effect of probe surface temperature on PIP required to remove deposits containing 5 and 10 $_{mole}$% CL/(Na+K), with no potassium and no carbonate [55].

Appendix A

Composition of different coal ash samples, investigated by Nowok [15]

Name	SiO_2	Al_2O_3	Fe_2O_3	TiO_2	CaO	MgO	Na_2O	K_2O	P_2O_5
Illionis No. 6 B/A* = 0.09	50.7	18.7	21.3	0.7	5.3	0.8	0.6	1.8	0.1
Pittsburgh No. 8 B/A = 0.10	50.8	20.2	17.5	1.3	5.2	1.3	0	2.5	0.2
Montana subbituminous B/A = 0.28	47.2	24.0	5.4	1.1	15.5	4.7	0.7	0.7	0.7
Beulah B/A = 0.83	27.5	14.2	9.9	2.8	27.4	5.9	10.8	1.0	0.4

$$* \frac{B}{A} = \frac{Na_2O + K_2O + CaO + MgO}{SiO_2 + Al_2O_3 + Fe_2O_3 + TiO_2}$$

Composition of five precipitator dusts from the recovery boiler, investigated by Piroozmand et al. [7]

Name	Na, $_{wt}\%$	K, $_{wt}\%$	Cl, $_{wt}\%$	SO_4, $_{wt}\%$	CO_3, $_{wt}\%$	Cl/(Na+K), $_{mole}\%$	K/(Na+K), $_{mole}\%$
A	28.8	6.5	2.0	58.2	2.5	2.6	11.7
B	30.8	6.4	3.3	46.3	11.3	4.0	10.9
C	32.4	4.1	11.9	43.4	4.3	13.6	6.9
D	31.6	3.7	10.4	50.7	0.6	12.2	6.4
E	24.7	11.2	0	62.5	0	12.2	21.1

Composition of coal ash slags, investigated by Wain et al. [5]

	SiO_2	Al_2O_3	FeO	CaO	MgO	TiO_2	Na_2O	K_2O	MnO	P_2O_5
A	54.0	24.2	11.1	2.4	2.5	0.9	1.0	3.7	0.1	0.1
B	57.6	28.2	5.8	2.2	1.4	1.9	0.7	1.3	-	0.4
C	52.8	24.2	12.6	3.2	1.8	1.1	0.6	3.6	0.2	-
D	53.1	25.6	8.6	4.9	2.1	0.7	1.6	2.9	0.2	0.2
E	51.7	27.5	10.8	3.9	1.3	1.0	0.8	2.9	0.2	0.1
F	51.8	27.3	11.2	1.8	1.3	1.0	3.5	1.2	-	0.5
G	51.7	24.1	11.6	5.0	1.9	1.2	1.1	3.1	-	0.4
H	43.5	18.2	22.6	9.3	2.4	0.9	0.9	2.0	-	0.2
I	52.3	25.4	10.7	2.0	1.7	1.0	1.8	5.0	-	0.2
J	49.2	25.1	13.9	4.7	2.2	1.0	1.1	2.6	0.1	0.1

Selected physical properties and thermal shock parameters (R, R') of boiler coal ash slags, investigated by Wain et al. [5]

	Porosity, $_{vol}\%$	Thermal expansion coefficient, 10^{-6}°C	σ_o, MN/m^{2} *	n*	R, °C	R',W/m
A	10	6.0	-	-	560	880
B	2	6.5	-	-	850	1170
C	5	6.3	440	8	840	-
D	35	5.9	1300	9	910	1110
E	4	5.3	1280	25	990	1420
F	25	7.1	690	7	620	960
G	38	6.1	500	7	880	1100
H	45	6.5	2780	10	750	1180
I	40	6.6	220	6	390	300
J	20	6.2	355	4	1170	1630

* σ_o and n have been calculated from the equ. (23), using experimental data.

Composition and characteristics of coal ash deposits, invstigated by Rezaei et al. [54]

Sample	SiO_2	Al_2O_3	Fe_2O_3	CaO	MgO	K_2O	Na_2O	TiO_2	SO_3
C	25.51	17.8	6.76	27.32	5.92	0.35	2.24	1.20	8.64

Sample	d_p [μm]	**Initial deformation temperature, °C**	**Spherical temperature, °C**	**Hemispherical temperature, °C**	**Fusion temperature, °C**	**Initial sintering temperature, °C**
C	<5-8 (50-70%)	1220	1250	1270	1600	670